mice on day 16 after the virus inoculation, if one copy of proviral DNA was postulated to reside in one $CD4^+$ cell.

One of us (Y.K.) previously attempted to investigate the mechanism of $CD4^+$ cell depletion seen in individuals with HIV-1 infection by employing a PBMC-transplanted NOD (NOD/Shi) *scid/scid* mouse system (24). Massive apoptosis was observed in HIV-1-uninfected $CD4^+$ cells in the spleens of the HIV-1-infected NOD-*scid/scid* mice. A combination of terminal deoxynucleotidyl transferase-mediated dUTP nick-end labeling and immunostaining for death-inducing tumor necrosis factor (TNF) family molecules showed that apoptotic cells were frequently found in conjugation with TNF-related apoptosis-inducing ligand (TRAIL)-expressing $CD3^+$ $CD4^+$ human T cells. Further observation that a neutralizing anti-TRAIL antibody inhibited the development of $CD4^+$ cell apoptosis suggested that a large number of HIV-1-uninfected $CD4^+$ cells undergo TRAIL-mediated apoptosis, contributing to the marked depletion of $CD4^+$ cells (24). The observation by Miura and his colleagues that the number of TRAIL-positive cells was consistently higher in HIV-1-infected mice than in uninfected ones makes it apparent that TRAIL expression is induced upon HIV-1 infection (23, 24). In this regard, the present observation that AK602 and ddI potently blocked the decrease in $CD4^+$ cells in spite of the rather increasing HIV-1 viremia in the face of AK602 or ddI (Fig. 7) suggests that the mere presence of viremia might not be sufficient for the HIV-induced apoptosis in $CD4^+$ cells. Our observation that most surviving $CD4^+$ cells in mice receiving AK602 or ddI were free of HIV-1 (see above) suggests that these anti-HIV-1 agents might block not only de novo HIV-1 infection, but also bystander killing of uninfected $CD4^+$ cells. The present data also suggest that a certain factor(s) such as cytokines produced by the freshly HIV-1-infected cells might mediate the apoptosis of bystander $CD4^+$ cells through the upregulation of TRAIL expression, death receptors (e.g., DR4 and DR5), and/or downregulation of decoy receptors (e.g., DcR1 and DcR2) (26, 27). However, experiments with a combination of terminal deoxynucleotidyl transferase-mediated dUTP nick-end labeling and TNF family molecules have to be conducted for better understanding of the bystander killing in regard to AK602's effects.

It is of note that several CCR5 antagonists are currently in various stages of development. AK602 has recently been administered to healthy adult subjects in a phase I clinical trial and shown to bind to CCR5 for an extended period of time, suggesting that an oral formulation with fewer administrations and lower dosage is possible for AK602 as a therapeutic agent for HIV-1 infection (J. Demarest, K. Adkison, S. Sparks, A. Shachoy-Clark, K. Schell, S. Reddy, L. Fang, K. O'Mara, S. Shibayama, and S. Piscitelli, 11th Conf. Retrovir. Opp. Infect., abstr. 139, 2004). Taken together, our observations that plasma viral load reached $\sim 10^6$ RNA copies/ml and that AK602 potently inhibited the replication of R5 HIV-1 strongly suggest that the present hu-PBMC-NOG mouse AIDS model could serve as a useful instrument for analyzing the pathogenesis of HIV-1 infection and testing the efficacy of antiviral agents.

ACKNOWLEDGMENTS

We thank Seth Steinberg for statistical analysis and Naoko Misawa, Yuji Kawano, and Hiromi Ogata for technical assistance and discussion.

This work was supported in part by grant-in-aids for Scientific Research on Priority Areas (14207025 and 15019086) from the Japanese Ministry of Education, Science, Sports, Culture and Technology of Japan (Monbu-Kagakusho) and a grant for AIDS Research (H15-AIDS-001) from the Ministry of Health, Labor, and Welfare of Japan (Kosei-Rohdosho).

REFERENCES

1. **Baba, M., O. Nishimura, N. Kanzaki, M. Okamoto, H. Sawada, Y. Iizawa, M. Shiraishi, Y. Aramaki, K. Okonogi, Y. Ogawa, K. Meguro, and M. Fujino.** 1999. A small-molecule, nonpeptide CCR5 antagonist with highly potent and selective anti HIV-1 activity. Proc. Natl. Acad. Sci. USA **96:**5698–5703.
2. **Carr, A., K. Samaras, A. Thorisdottir, G. R. Kaufmann, D. J. Chisholm, and D. A. Cooper.** 1999. Diagnosis, prediction, and natural course of HIV-1 protease-inhibitor associated lipodystrophy, hyperlipidaemia, and diabetes mellitus: a cohort study. Lancet **353:**2093–2099.
3. **Dean, M., M. Carrington, C. Winkler, G. A. Huttley, M. W. Smith, R. Allikmets, J. J. Goedert, S. P. Buchbinder, E. Vittinghoff, E. Gomperts, S. Donfield, D. Vlahov, R. Kaslow, A. Saah, C. Rinaldo, R. Detels, and S. J. O'Brien.** 1996. Genetic restriction of HIV-1 infection and progression to AIDS by a deletion allele of the CKR5 structural gene. Hemophilia Growth and Development Study, Multicenter AIDS Cohort Study, Multicenter Hemophilia Cohort Study, San Francisco City Cohort, ALIVE Study. Science **273:**1856–1862.
4. **Easterbrook, P. J.** 1999. Long-term non-progression in HIV infection: definitions and epidemiological issues. J. Infect. **38:**71–73.
5. **Fauci, A. S.** 1999. The AIDS epidemic—considerations for the 21st century. N. Engl. J. Med. **341:**1046–1050.
6. **Finzi, D., J. Blankson, J. D. Siliciano, J. B. Margolick, K. Chadwick, T. Pierson, K. Smith, J. Lisziewicz, F. Lori, C. Flexner, T. C. Quinn, R. E. Chaisson, E. Rosenberg, B. Walker, S. Gange, J. Gallant, and R. F. Siliciano.** 1999. Latent infection of CD4+ T cells provides a mechanism for lifelong persistence of HIV-1, even in patients on effective combination therapy. Nat. Med. **5:**512–517.
7. **Gartner, S., P. Markovits, D. M. Markovitz, M. H. Kaplan, R. C. Gallo, and M. Popovic.** 1986. The role of mononuclear phagocytes in HTLV-III/LAV infection. Science **233:**215–219.
8. **Garaci, E., S. Aquaro, C. Lapenta, A. Amendola, M. Spada, S. Covaceuszach, C. F. Perno, and F. Belardelli.** 2003. Anti-nerve growth factor Ab abrogates macrophage-mediated HIV-1 infection and depletion of CD4+ T lymphocytes in hu-SCID mice. Proc. Natl. Acad. Sci. USA **100:**8927–8932.
9. **Ichiyama, K., S. Yokoyama-Kumakura, Y. Tanaka, R. Tanaka, K. Hirose, K. Bannai, T. Edamatsu, M. Yanaka, Y. Niitani, N. Miyano-Kurosaki, H. Takaku, Y. Koyanagi, and N. Yamamoto.** 2003. A duodenally absorbable CXC chemokine receptor 4 antagonist, KRH-1636, exhibits a potent and selective anti-HIV-1 activity. Proc. Natl. Acad. Sci. USA **100:**4185–4190.
10. **Ito, M., H. Hiramatsu, K. Kobayashi, K. Suzue, M. Kawahata, K. Hioki, Y. Ueyama, Y. Koyanagi, K. Sugamura, K. Tsuji, T. Heike, and T. Nakahata.** 2002. NOD/SCID/γ(c)(null) mouse: an excellent recipient mouse model for engraftment of human cells. Blood **100:**3175–3182.
11. **Kavlick, M. F., and H. Mitsuya.** 2001. The emergence of drug resistant HIV-1 variants and its impact on antiretroviral therapy of HIV-1 infection, p. 279–312. *In* E. De Clercq (ed.), The art of antiretroviral therapy. American Society for Microbiology, Washington, D.C.
12. **Koh, Y., H. Nakata, K. Maeda, H. Ogata, G. Bilcer, T. Devasamudram, J. F. Kincaid, P. Boross, Y. F. Wang, Y. Tie, P. Volarath, L. Gaddis, R. W. Harrison, I. T. Weber, A. K. Ghosh, and H. Mitsuya.** 2003. Novel bis-tetrahydrofuranylurethane-containing nonpeptidic protease inhibitor (PI) UIC-94017 (TMC114) with potent activity against multi-PI-resistant human immunodeficiency virus in vitro. Antimicrob. Agents Chemother. **47:**3123–3129.
13. **Koyanagi, Y., S. Miles, R. T. Mitsuyasu, J. E. Merrill, H. V. Vinters, and I. S. Chen.** 1987. Dual infection of the central nervous system by AIDS viruses with distinct cellular tropisms. Science **236:**819–822.
14. **Koyanagi, Y., Y. Tanaka, J. Kira, M. Ito, K. Hioki, N. Misawa, Y. Kawano, K. Yamasaki, R. Tanaka, Y. Suzuki, Y. Ueyama, E. Terada, T. Tanaka, M. Miyasaka, T. Kobayashi, Y. Kumazawa, and N. Yamamoto.** 1997. Primary human immunodeficiency virus type 1 viremia and central nervous system invasion in a novel hu-PBL-immunodeficient mouse strain. J. Virol. **71:**2417–2424.
15. **Lee, B., M. Sharron, L. J. Montaner, D. Weissman, and R. W. Doms.** 1999. Quantification of CD4, CCR5, and CXCR4 levels on lymphocyte subsets, dendritic cells, and differentially conditioned monocyte-derived macrophages. Proc. Natl. Acad. Sci. USA **96:**5215–5220.
16. **Lyons, A. B.** 2000. Analysing cell division in vivo and in vitro using flow cytometric measurement of CFSE dye dilution. J. Immunol. Methods **243:**147–154.
17. **Maeda, K., K. Yoshimura, S. Shibayama, H. Habashita, H. Tada, K. Sagawa, T. Miyakawa, M. Aoki, D. Fukushima, and H. Mitsuya.** 2001. Novel low molecular weight spirodiketopiperazine derivatives potently inhibit R5

HIV-1 infection through their antagonistic effects on CCR5. J. Biol. Chem. **276:**35194–35200.

18. **Maeda, Y., M. Foda, S. Matsushita, and S. Harada.** 2000. Involvement of both the V2 and V3 regions of the CCR5-tropic human immunodeficiency virus type 1 envelope in reduced sensitivity to macrophage inflammatory protein 1α. J. Virol. **74:**1787–1793.
19. **McCune, J. M., R. Namikawa, C. C. Shih, L. Rabin, and H. Kaneshima.** 1990. Suppression of HIV infection in AZT-treated SCID-hu mice. Science **247:**564–566.
20. **Mitsuya, H., and S. Broder.** 1986. Inhibition of the in vitro infectivity and cytopathic effect of human T-lymphotropic virus type III/lymphadenopathy virus-associated virus (HTLV-III/LAV) by 2′,3′-dideoxynucleosides. Proc. Natl. Acad. Sci. USA **83:**1911–1915.
21. **Mitsuya, H., and S. Broder.** 1987. Strategies for antiviral therapy in AIDS. Nature **325:**773–778.
22. **Mitsuya, H., and J. Erickson.** 1999. Discovery and development of antiretroviral therapeutics for HIV infection, p. 751–780. *In* T. C. Merigan, J. G. Bartlet, and D. Bolognesi (ed.), Textbook of AIDS medicine. Williams & Wilkins, Baltimore, Md.
23. **Miura, Y., N. Misawa, Y. Kawano, H. Okada, Y. Inagaki, N. Yamamoto, M. Ito, H. Yagita, K. Okumura, H. Mizusawa, and Y. Koyanagi.** 2003. Tumor necrosis factor-related apoptosis-inducing ligand induces neuronal death in a murine model of HIV central nervous system infection. Proc. Natl. Acad. Sci. USA **100:**2777–2782.
24. **Miura, Y., N. Misawa, N. Maeda, Y. Inagaki, Y. Tanaka, M. Ito, N. Kayagaki, N. Yamamoto, H. Yagita, H. Mizusawa, and Y. Koyanagi.** 2001. Critical contribution of tumor necrosis factor-related apoptosis-inducing ligand (TRAIL) to apoptosis of human CD4+ T cells in HIV-1-infected hu-PBL-NOD-SCID mice. J. Exp. Med. **193:**651–660.
25. **Mosier, D. E., R. J. Gulizia, S. M. Baird, D. B. Wilson, D. H. Spector, and S. A. Spector.** 1991. Human immunodeficiency virus infection of human-PBL-SCID mice. Science **251:**791–794.
26. **Pan, G., J. Ni, Y. F. Wei, G. Yu, R. Gentz, and V. M. Dixit.** 1997. An antagonist decoy receptor and a death domain-containing receptor for TRAIL. Science **277:**815–818.
27. **Pan, G., K. O'Rourke, A. M. Chinnaiyan, R. Gentz, R. Ebner, J. Ni, and V. M. Dixit.** 1997. The receptor for the cytotoxic ligand TRAIL. Science **276:**111–113.
28. **Ratain, M., and W. Plunkett.** 1997. Pharmacology, p. 875–889. *In* J. Holland, R. Bast, Jr., D. Morton, E. Frei, D. KuFe, and R. Weichselbaum (ed.), Cancer medicine, 4th ed. Williams and Wilkins, Baltimore, Md.
29. **Ruxrungtham, K., E. Boone, H. Ford, Jr., J. S. Driscoll, R. T. Davey, Jr., and H. C. Lane.** 1996. Potent activity of 2′-β-fluoro-2′,3′-dideoxyadenosine against human immunodeficiency virus type 1 infection in hu-PBL-SCID mice. Antimicrob. Agents Chemother. **40:**2369–2374.
30. **Strizki, J. M., S. Xu, N. E. Wagner, L. Wojcik, J. Liu, Y. Hou, M. Endres, A. Palani, S. Shapiro, J. W. Clader, W. J. Greenlee, J. R. Tagat, S. McCombie, K. Cox, A. B. Fawzi, C. C. Chou, C. Pugliese-Sivo, L. Davies, M. E. Moreno, D. D. Ho, A. Trkola, C. A. Stoddart, J. P. Moore, G. R. Reyes, and B. M. Baroudy.** 2001. SCH-C (SCH 351125), an orally bioavailable, small molecule antagonist of the chemokine receptor CCR5, is a potent inhibitor of HIV-1 infection in vitro and in vivo. Proc. Natl. Acad. Sci. USA **98:**12718–12723.
31. **Walker, U. A., B. Setzer, and N. Venhoff.** 2002. Increased long-term mitochondrial toxicity in combinations of nucleoside analogue reverse-transcriptase inhibitors. AIDS **16:**2165–2173.
32. **Westervelt, P., H. E. Gendelman, and L. Ratner.** 1991. Identification of a determinant within the human immunodeficiency virus 1 surface envelope glycoprotein critical for productive infection of primary monocytes. Proc. Natl. Acad. Sci. USA **88:**3097–3101.
33. **Yahata, T., K. Ando, Y. Nakamura, Y. Ueyama, K. Shimamura, N. Tamaoki, S. Kato, and T. Hotta.** 2002. Functional human T lymphocyte development from cord blood CD34+ cells in nonobese diabetic/Shi-scid, IL-2 receptor gamma null mice. J. Immunol. **169:**204–209.
34. **Yoshida, A., R. Tanaka, T. Murakami, Y. Takahashi, Y. Koyanagi, M. Nakamura, M. Ito, N. Yamamoto, and Y. Tanaka.** 2003. Induction of protective immune responses against R5 human immunodeficiency virus type 1 (HIV-1) infection in hu-PBL-SCID mice by intrasplenic immunization with HIV-1-pulsed dendritic cells: possible involvement of a novel factor of human CD4(+) T-cell origin. J. Virol. **77:**8719–8728.
35. **Yoshimura, K., R. Kato, K. Yusa, M. F. Kavlick, V. Maroun, A. Nguyen, T. Mimoto, T. Ueno, M. Shintani, J. Falloon, H. Masur, H. Hayashi, J. Erickson, and H. Mitsuya.** 1999. JE-2147: a dipeptide protease inhibitor (PI) that potently inhibits multi-PI-resistant HIV-1. Proc. Natl. Acad. Sci. USA **96:**8675–8680.

Rev. Med. Virol. 2005; **15**: 169–178.
Published online 11 March 2005 in Wiley InterScience (www.interscience.wiley.com).
Reviews in Medical Virology **DOI**: 10.1002/rmv.462

REVIEW

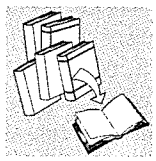

Death ligand-mediated apoptosis in HIV infection

Yoshiharu Miura* and Yoshio Koyanagi

Laboratory of Viral Pathogenesis, Research Center for AIDS, Institute for Virus Research, Kyoto University, Japan

SUMMARY

Apoptosis has been suggested to cause severe $CD4^+$ T cell depletion in patients infected with HIV. This review focuses on the biological events involved in death ligand-induced apoptosis during HIV infection. Among these ligands, TRAIL appears critical in HIV-infection. Death ligand-induced apoptosis might be a major pathogenic event in many virus-induced diseases including AIDS and the clarification of its mechanism will aid in the development of therapeutic strategies. Copyright © 2005 John Wiley & Sons, Ltd.

Received: 12 November 2004; Accepted: 15 November 2004

INTRODUCTION

Severe CD4 depletion is a hallmark of acquired immunodeficiency syndrome (AIDS) and the gradual loss of $CD4^+$ T cells leading to the onset of AIDS appears to be a result of infection with human immunodeficiency virus (HIV). Apoptosis, which has been shown to be significantly induced in HIV-infected individuals, seems to trigger the CD4 depletion during disease progression. Two major pathways have been identified from extensive molecular biology-based analysis; an extrinsic pathway, which is initiated by the binding of tumor-necrosis factor (TNF) family ligands to their cognate death receptors, and an intrinsic pathway, which is initiated by an internal sensor system that mainly transmits signals to the mitochondria and is mediated by Bcl-2-related proteins [1,2]. This review summarises our present level of understanding of the molecular mechanisms behind the extrinsic pathway of T lymphocyte apoptosis with HIV infection.

Corresponding author: Dr Y. Miura, Institute for Virus Research, Kyoto University, 53 Shougoin-kawaramachi, Sakyou-ku, Kyoto 606-8507, Japan. E-mail: ymiura@virus.kyoto-u.ac.jp

Abbreviations used
AICD, activation-induced cell death; AIDS, acquired immunodeficiency syndrome; cFLIP, cellular FLICE inhibitory protein; DISC, death-inducing signaling complex; FADD, Fas-associated death domain; FLICE, FADD-like ICE; HIV, human immunodeficiency virus; TNF, tumor necrosis factor; TRAIL, TNF-related apoptosis-inducing ligand.

HIV INFECTION AND APOPTOSIS

Apoptosis is thought to occur in HIV-infected individuals and arise from the following mechanisms; HIV-induced syncytium formation, HIV protein-induced cell death, activation-induced cell death (AICD) and bystander cell killing (Figure 1). Ballooning cells and multinucleic giant cells are frequently found in virus-infected cell cultures *in vitro*. The cytopathic effect (CPE) in HIV-infected $CD4^+$ T cell cultures is known to be the formation of syncytia between productively infected and adjacent uninfected cells and clearly induces the apoptosis in these cells, obviously dependent on viral replication [3,4]. Syncytia are also found in infected tissues [5,6]. The envelope glycoprotein complex of gp120-gp41 on the surface of the infected cells, which causes the death of both infected and adjacent uninfected cells, seems to be one of the dominant apoptosis-inducing molecules encoded by the HIV-1 genome (Figure 2). The envelope expressed on the plasma membrane of infected cells can interact with the CD4 molecule and a suitable co-receptor to trigger cell-to-cell fusion; resulting in syncytia and subsequently apoptosis [7,8]. It was reported that mitochondria-dependent apoptosis (intrinsic pathway) occurs with the fusion of envelope-expressing cells with CD4- and coreceptor-expressing target cells [9]. The shedding of HIV-encoded proteins such as envelope, Tat and Vpr (Figure 2) has also been shown to trigger apoptosis in both infected and

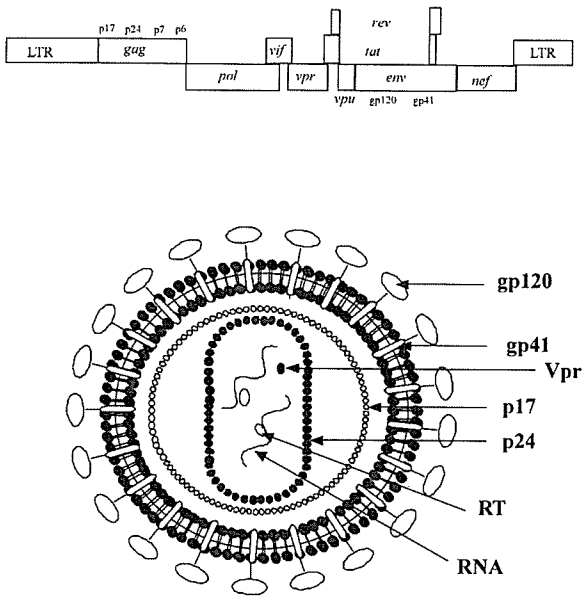

Figure 1. The HIV-1 provirus and its proteins. Gag and Gag-Pol polyprotein precursors are processed by the viral protease into nine subunits: protease, reverse transcriptase, integrase, matrix, capsid, p2, nucleocapsid, p1 and p6. Env is cleaved by cellular proteases, such as furin, into surface gp120 and transmembrane gp41 moieties. Tat is a transcriptional and translational regulator of expression. The RNA target region, the transactivation response (TAR) element, is located at the 5′ end of all viral transcripts. Rev has a major role in the nuclear-export of large HIV-1 RNA (gag and env transcripts) and regulates the shift between early and late viral gene expression. The viral-infectivity factor (Vif), viral protein u (Vpu), viral protein R (Vpr) and negative effector (Nef) proteins are known as accessory proteins because they are dispensable for viral growth in some cell-culture systems

uninfected cells in culture. Tat effectively induces apoptosis by downregulating the expression of Bcl-2 and upregulating the expression of Bax as well as caspase 8 [10,11]. On the other hand, the typical intrinsic pathway can be triggered by the soluble form of Vpr protein, which causes a rapid disintegration of the mitochondrial transmembrane potential in intact cells, as well as the release of cytochrome c and subsequent apoptosis [12]. On the other hand, AICD, which is known to be dependent on death receptors, was observed in *ex vivo* cultured T cells from HIV-infected patients following activation with mitogens, superantigens or antibodies specific for TCR [13]. AICD was originally found to occur during the elimination of prolongly activated T cells when the inflammatory reaction is coming to an end. Significantly, increased destruction of $CD4^+$ T cells in secondary lymphoid organs such as lymph nodes and spleen has been reported in HIV-infected individuals [14]. In addition, it has been postulated that HIV-1 infection causes uninfected $CD4^+$ T cells to die, and a bystander cell killing mechanism has been suggested based on histopathological analyses of lymph nodes in HIV-1-infected individuals and simian immunodeficiency virus (SIV)-infected monkeys [15]. The persistent existence of HIV proteins (Tat, gp120, Nef, Vpu) *in vivo* might stimulate apoptosis in uninfected bystander cells.

APOPTOSIS AND DEATH LIGAND

The extrinsic pathway arises from the binding of the ligand molecule to its respective membrane-bound death receptor and the engagement of the caspase cascade (Figure 3). Death receptors are members of the TNF receptor superfamily, which initiate a rapid activation of the caspase cascade and commit the cell to apoptosis when triggered by their cognate TNF family ligands. These ligands include Fas ligand (FasL), TNF, TNF-related apoptosis-inducing ligand (TRAIL) and TWEAK, and all of the death receptors possess both a cysteine-rich extracellular domain and an intracellular cytoplasmic sequence motif, known as the death domain (DD).

FasL is a type 2 membrane protein and an exclusive ligand for Fas, inducing Fas-mediated apoptosis [16]. The ligation of FasL to Fas triggers the Fas monomers to combine into trimeric Fas-complexes (Figure 3). The intracellular domain of Fas contains the DD, a stretch of 80 amino acids. After the trimerisation of Fas molecules, the DD recruits many cytosol proteins and forms a multi-protein death-inducing signaling complex (DISC) [17,18]. Immediately following Fas/FasL ligation, the prompt recruitment of a serine-phosphorylated adaptor molecule, Fas-associated DD (FADD), is induced and then the Fas/FADD interaction is coordinated through the highly conserved DD motifs found in both proteins. FADD serves as a bridge between Fas and downstream molecules, such as Fas-like IL-1β converting enzyme (FLICE) as well as cytotoxicity-dependent APO-1-associated protein 3 (CAP3). The FADD-FLICE/CAP3 interaction allows the liberation of caspase 8 and CAP3 in an active form from their dormant states. Formation of the DISC, which is composed of Fas, FADD and FLICE/CAP3, results in the initiation of a signal cascade to downstream target molecules, such as procaspase 3, 6 and 7. The activated

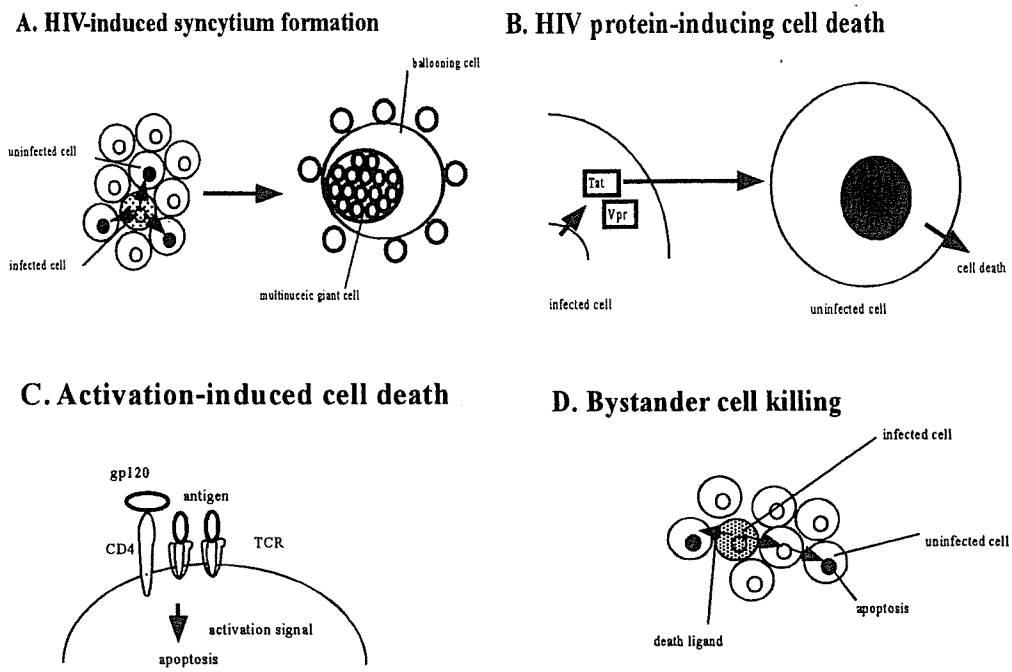

Figure 2. Mechanism of HIV-1-induced cell death. (A) HIV-induced syncytium formation arising from cell to cell fusion. (B) HIV protein-induced cell death. (C) Activation induced cell death through stimulation of TCR or gp120. (D) Bystander cell killing mediated by the death signal

form of caspase 3 efficiently cleaves a variety of cellular constituents, including the DNA repair enzymes, poly-ADP ribose polymerase and DNA-induced protein kinase, cytoskeletal proteins, lamins and actin, and the endonuclease modulator, caspase-activated deoxyribonuclease (CAD) inhibitor (ICAD) [19]. During Fas-mediated apoptosis, the concomitant activation of many other proteins appears to occur. Receptor-interacting protein (RIP), RIP-associated ICH/CED-3-homologous protein with a DD (RAIDD), and procaspase 2 from part of another signaling cascade of the Fas-mediated death pathway were shown to be activated [20]. The activation of the RIP-RAIDD arm of the cell death machinery was demonstrated to serve as a co-stimulator of the FADD-FLICE system [19]. Moreover, upregulation of cytoplasmic DAXX, leading to induction of the stress-activated protein kinase/c-Jun *N*-terminal kinase (SAP/JNK) pathway, represents yet another mechanism by which Fas-mediated apoptosis may occur [21]. The activated form of caspases executes the apoptotic process by cleaving various intracellular substrates leading to genomic DNA fragmentation and resulting in cell membrane blebbing and the exposure of phagocytosis signaling molecules on the cell surface. As mentioned above, FasL-dependent apoptosis plays a critical role in the peripheral elimination of prolongly activated lymphocytes at the end of an immune response [22,23]. Thus, it may be true that FasL has a central role in many of the biological phenomena of activation-induced T-cell apoptosis. In fact, *gld* mice that carry hereditary mutations in the genes encoding FasL are found to suffer from accumulating lymphocytes and a lethal enlargement of lymph nodes. These findings indicate that the main biological role of FasL is to signal the Fas^+ cells to induce instructive apoptosis during the peripheral elimination of lymphocytes. FasL is also expressed in immuno-privileged tissue in which it is difficult to elicit an inflammatory response such as testis and eye [24,25]. FasL may also act as a barrier in the vessel [26]. Significant expression was found on vascular endothelial cells, where it may prevent leukocyte exfiltration into non-inflamed tissues, again by triggering the apoptosis of Fas-expressing leukocytes [27].

TNF, first identified in 1975, is a conventional cytokine and representative of a large superfamily of cytokines that exert physiological roles in cell proliferation, cell death and inflammation as well

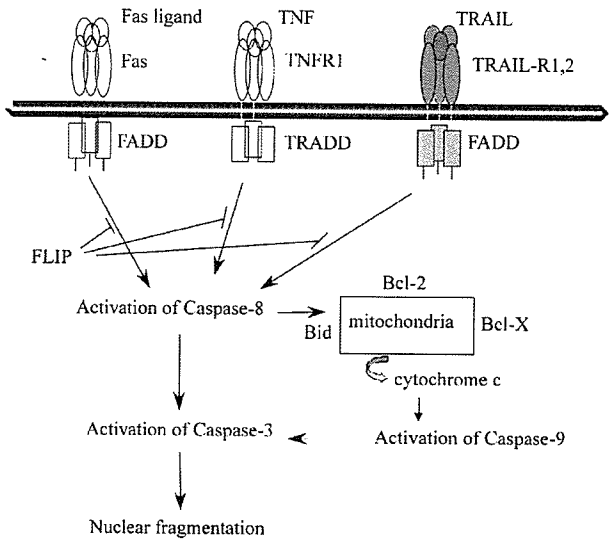

Figure 3. The death ligand-mediated apoptotic pathway. Ligation of the death ligand receptor leads to the formation of DISC comprising the adaptor protein (FADD, TRADD) and procaspase-8 and resulting in the activation of caspase-8. The binding of FLIP to FADD inhibits caspase-8 activation. Caspase-8 can then either directly activate effector caspases (caspase-3) or cleave the proapoptotic Bcl-2 family member Bid. Bid acts with the proapoptotic Bcl-2 family. The involvement of the mitochondria is manifested by the release of cytochrome c into the cytosol where it associates with Apaf-1 and procaspase-9 to form the apoptosome, leading to caspase-9 activation and subsequent caspase-3 activation and nuclear fragmentation

as pathological roles in immunological processes. The best-characterised death receptor is TNFR1. Trimerised TNFR1 can recruit an adaptor molecule, TNFR-associated DD (TRADD), which subsequently recruits FADD and procaspase-8. The intracellular signaling cascade through TNFR1 seems to be more complex than that through Fas. Indeed, in addition to recruiting caspase-activating adaptor molecules, TNFR1 induces the recruitment of many other proteins that engage various signal transduction pathways, some of which either abrogate or potentiate the apoptotic response. For example, TRADD also binds serine-threonine kinase RIP, thereby coupling the stimulation of TNFR1 to the activation of nuclear factor-κB (NF-κB) and offering protection against TNF-induced apoptosis [28]. RIP possesses a functional *N*-terminal kinase domain and can autophosphorylate itself, but this phospharylation does not induce activation of NF-κB. TNF receptor-associated factor 2 (TRAF2) has been likewise implicated in the activation of NF-κB through stimulation of NF-κB-inducing kinase (NIK). However, studies TRAF-2-knockout mice indicated that RIP is most likely responsible for the activation of NF-κB, whereas TRAF2 preferentially activates JNK. TNF knockout mice exhibited increased susceptibility to microbial infection and suppressed inflammatory response when challenged with bacterial endotoxin. These findings together with results obtained *in vitro* suggested that the main biological role of TNF is the induction of inflammatory-response and stress-response genes through the transcription factors AP-1 and NF-κB.

TRAIL was first identified in 1995 based on its sequence homology to other members of the TNF superfamily [29]. TRAIL is also a type 2 transmembrane protein and its highest level of homology is with FasL, exhibiting 28% amino acid identity in the extracellular receptor-binding motif. Two other unique characteristics of TRAIL have been identified. First, TRAIL selectively induces apoptosis both *in vitro* in transformed cells and *in vivo* in tumor cells but not in most normal cells, except thymocytes, neural cells and hepatocytes [30–32]. Second, whereas the expression of other members of the TNF family is tightly regulated and often only transiently induced on activated cells, the transcript of TRAIL was constitutively expressed in some tissues including spleen, lung and prostate [29]. Because the level of TRAIL expression is not consistent with numbers of apoptotic cells, it was assumed that the expression of its cognate receptor would be restricted or alternatively, that apoptosis in only limited cells would be induced under some biological conditions. However, the regulation of TRAIL-induced cell death appears to be more complex than initially thought because five receptors for TRAIL have been identified including two death-inducing receptors (DR4 and DR5), two decoy receptors (DcR1 and DcR2) [33,34], and the secreted TNFR homologue receptor osteoprotegerin [35,36]. The cytoplasmic region of two of these receptors, DR4 and DR5, contains a region with significant homology to the DD of TNFR1 and Fas, and it was confirmed that DR4 and DR5 are able to induce signals for apoptosis [37]. By contrast, DcR2 contains an incomplete DD and so is unable to transduce a death signal [38]. Similarly, DcR1, which unlike the others lacks a cytoplasmic domain and is bound to the cell surface via a glycosyl-phosphatidylinositol (GPI) anchor, does not mediate apoptosis upon ligation [39]. The

activation of caspase has been demonstrated in TRAIL-induced apoptosis *in vitro*. Many of the same caspases involved in Fas and TNF-induced apoptosis were shown to participate in the TRAIL-induced cell death. The activation of death-induced TRAIL-receptors (DR4 and DR5) initiates recruitment of FADD, which in turn directly recruits procaspase-8 to form DISC and results in autoactivation of caspase-8, which then activates downstream effector caspases or the cleaved RIP directly [40]. The NF-κB or JNK signaling pathway was also shown to be activated through DR4 and DR5, respectively, analogous to TNFR1 [41]. It has been suggested that decoy receptors operate to protect normal cells from TRAIL-mediated apoptosis [33,38]. Also, certain intracellular regulatory molecules that control TRAIL-induced apoptosis, such as cFLIP (cellular-FLICE-inhibitory protein), may also operate [42]. Early studies indicated a high level of cFLIP in a TRAIL-resistant melanoma cell line [43]. Furthermore, the level of cFLIP clearly correlated with the sensitivity to TRAIL in some keratinocytes [42]. In addition, it was shown that overexpression of cFLIP frequently causes cells to become resistant to TRAIL because in the presence of cFLIP, procaspase-8 is unable to convert processed caspase-8 generated at the DISC and so remains inactivated [44]. However, inhibition of overall transcription and translation was observed in TRAIL-induced apoptosis without a change in cFLIP levels [45]. These results suggest a significant role for cFLIP in modulating the sensitivity to TRAIL of many cells. It was recently reported that mice deficient in TRAIL exhibit defects of apoptosis in the thymus and develop heightened autoimmune responses, hypersensitivity, to collagen-induced arthritis and streptozotocin-induced diabetes [46]. However, the physiological defect was slighter in the TRAIL-deficient mice than either the FasL- or TNF-deficient mice. Thus, TRAIL seems to have minor physiological roles.

The screening of an EST database revealed another death ligand, called TWEAK [47], whose closest homologue is TNF. Like TNF, TWEAK efficiently promotes apoptosis in certain tumor cell lines and the inhibition of protein synthesis in TWEAK-induced cells further augments apoptosis. TWEAK efficiently activates NF-κB and induces expression of IL-8. Unlike TNF, whose expression is found in activated lymphoid and endothelial cells, the TWEAK transcript was found to be constitutively expressed in many tissues. DR3 was originally identified as a molecule interacting with TNFR1 and reported to be a receptor for TWEAK [48,49]. Similar to TNF-TNFR1 signaling, the activation of DR3 was demonstrated to induce apoptosis as well as the activation of NF-κB and the apoptosis is mediated via interactions with TRADD, FADD and caspase 8, while the activation of NF-κB is induced by a TRADD, TRAF2 and RIP-mediated pathway. However, a high level of TWEAK expression was found in many tissues, whereas DR3 expression was demonstrated to be restricted to peripheral blood lymphocytes (PBLs), thymus, spleen, colon and small intestine [50]. The physiological role of TWEAK remains to be elucidated.

HIV INFECTION AND DEATH LIGANDS

Extensive death ligand-mediated apoptosis is thought to occur in many infectious diseases. Significant augmentation of FasL expression is found in cells expressing hepatitis B and hepatitis C viruses [51,52], although some studies indicated that an increased level of FasL *in vivo* is not associated with HIV disease progression [53,54]. It is remarkable that HIV-1-infected T cells in culture as well as T cells from HIV-infected individuals are highly susceptible to Fas-induced apoptosis [55]. Clinical studies have shown that the expression of Fas as well as the susceptibility to Fas-induced apoptosis increased significantly in cultured $CD4^+$ and $CD8^+$ T cells derived from HIV-1-infected individuals and this high level of Fas expression was positively correlated with disease progression [56]. An increased level of soluble Fas was also found in the plasma of HIV-1-infected individuals and this can be used as a marker for the prognosis of AIDS [57]. FasL was also shown to be upregulated in cultured $CD4^+$ and $CD8^+$ T cells from AIDS patients and, a high level of soluble FasL in serum was found in AIDS patients. Furthermore, FasL expression on macrophages was detected in lymphoid tissue of HIV-1-infected subjects [58]. The observation that retinoic acid inhibits the expression of FasL and the subsequent apoptosis of $CD4^+$ T cells *ex vivo* further supports a causal role for Fas-FasL interactions in the $CD4^+$ T cell death that is induced by HIV infection [59]. Interestingly, the exposure of uninfected monocytes to HIV-1 particles *in vitro* has been

reported to enhance significantly FasL expression, suggesting that HIV-1 can induce Fas-dependent apoptosis through the interaction of monocytes with T cells [60,61]. Furthermore, the crosslinking of the CD4 molecule with HIV-1 gp120 on $CD4^+$ T cells activates the Fas-FasL pathway and Nef-expressing T cells co-express FasL, thereby becoming potential killer cells of uninfected Fas-expressing T cells [62,63]. Similarly, Tat, which is secreted by HIV-infected cells, was shown to upregulate Fas and FasL expression on uninfected cells and enhance their susceptibility to Fas-induced apoptosis [61,64]. Since it is known to be expressed even before integration, Nef may protect infected cells from apoptosis and permit infection in resting cells. Interestingly, significant protection against apoptosis is provided through the downregulation of ASK-1 signaling by Fas-FasL suggesting that Nef acts as an anti-apoptotic protein in the infected cells during its replication [65]. It is also clear that Vpu enhances susceptibility to Fas-induced apoptosis [66]. However, the possible involvement of the Fas/FasL pathway in AICD of $CD4^+$ T cells from HIV-1-infected individuals [67,68] remains controversial. Katsikis *et al.* reported that the AICD cultured $CD4^+$ T cells from HIV-infected patients was Fas-independent [69] and it was shown that neither Fas protein nor biologically active FasL was detectable at significant levels in freshly isolated T cells from HIV-1-infected individuals [54]. In addition, FasL-mediated apoptosis may contribute to the elimination of virus-infected cells by the virus-specific cytotoxic lymphocytes or NK cells [70,71].

Susceptibility to TNF in $CD4^+$ T cells isolated from HIV-infected individuals has also been investigated extensively. Although an early report found that peripheral blood T cells from HIV-positive patients were resistant to apoptosis that was induced by ligation of TNFR [56], a more recent study showed that both $CD4^+$ and $CD8^+$ T cells from HIV-infected individuals were significantly susceptible to TNFR1- and R2-induced apoptosis [72]. The possible contribution of TNFR-mediated apoptosis to $CD8^+$ T cell depletion was implied from the observation that ligation of Env to the CXCR4 coreceptor upregulated the expression of TNFR2 on $CD8^+$ T cells, which became susceptible to death induced by the membrane-bound form of TNF expressed on macrophages [73]. An increased level of TNF was also detected in the serum of symptomatic individuals and clearly high levels of soluble TNFR2 were found to be predictive of HIV disease progression [74].

HIV INFECTION AND TRAIL

Treatment with interferon (IFN) significantly augmented the expression of TRAIL on $CD4^+$ T cells [75], monocytes [76] and dendritic cells (DC) [77]. In addition, infection with measles virus augmented TRAIL expression on DC [78]. Therefore, it is possible that TRAIL is involved in the pathogenesis of HIV. In fact, TRAIL, but not FasL-dependent AICD, was detected in $CD4^+$ T cells isolated from HIV-1-infected individuals *in vitro* [79,80]. TRAIL might contribute to a constructive apoptosis of virus-infected cells because T cells from HIV-1-infected patients were more susceptible to the induction of apoptosis by this ligand than uninfected cells, suggesting that TRAIL is involved in HIV-associated T-cell apoptosis [79]. In fact, AICD in $CD4^+$ T cells isolated from HIV-1-infected individuals was inhibited by antagonistic TRAIL-specific antibodies [80]. Furthermore, using an HIV-1-infected mouse model, a significant level of TRAIL-dependent apoptosis in uninfected $CD4^+$ T cells was found. The spleen tissue of hu-PBL-NOD-SCID mice was investigated following infection with HIV-1 and large numbers of $TUNEL^+$ $CD4^+$ cells were found mainly in uninfected cells. The number of $TUNEL^+$ cells was clearly inhibited after administration of anti-TRAIL but not anti-FasL antibody, suggesting that TRAIL is a major death ligand in HIV-1-infected tissues [81,82]. Following infection with HIV-1, Tat protein is released by macrophages or monocytes and seems to upregulate the expression of TRAIL on macrophages as shown by Zhang, indicating that TRAIL-dependent cell death occurs in bystander $CD4^+$ T cells, perhaps triggered by Tat produced from HIV-1-infected cells [83,84].

It is likely that TRAIL is primarily responsible for the apoptosis of bystander $CD4^+$ T cells in HIV-infected lymphoid organs. However, several issues remain to be resolved. First, the mechanism by which HIV-1 infection induces the expression of TRAIL in $CD4^+$ T cells remains to be determined. It was found that the number of $TRAIL^+$ cells was consistently higher in HIV-1-infected mice than uninfected mice. A similar upregulation of TRAIL expression with HIV-1 infection was observed especially on HIV-1-infected

macrophages [85]. The expression of TRAIL on T cells is induced by a variety of stimuli, including type I IFNs and TCR-mediated signals [75,86,87]. Thus it can be postulated that TRAIL was induced to express on HIV-1-uninfected $CD4^+$ T cells by viral or cellular factors from either HIV-1-infected or bystander cells in HIV-1-infected lymphoid organs. Second, it is necessary to determine the receptor molecule involved in TRAIL-mediated apoptosis. It is not yet clear which receptor contributes to this phenomenon. In other viral infections, viral proteins regulate the expression of these receptors. In adenovirus, E3 downregulates its receptor DR4 and DR5 [88]. In respiratory syncytial virus, infection strongly upregulated DR4 and DR5 expression [89]. In HIV infection, Tat and gp120 seem to upregulate DR4 and DR5 expression.

TRAIL seems to be one of the most significant molecules in HIV infection [81,85,90]. This ligand was predominantly expressed on macrophages and monocytes after HIV-1 infection, and was able to induce apoptosis in neurons *in vitro* and *in vivo*, which might explain the neuronal death in HIV-encephalopathy. Recently, a murine model of HIV-encephalopathy was developed and it was found that neuronal apoptosis was significantly induced by TRAIL expressed on HIV-infected macrophages [85]. Furthermore, neuronal apoptosis was confirmed in the brain tissue of HIV-1-encephalopathy patients and cells cultured *in vitro* [90,91]. It is possible that TRAIL has a central role in disease progression in some virus-induced diseases.

CONCLUSION

Although the mechanism of the apoptosis in HIV-infected individuals is likely to be multifactorial, its induction is a critical event *in vivo*. The death ligands in HIV infection are important for this apoptosis in addition to mitochondria-mediated apoptosis. A novel immune-based therapy for modulating the apoptosis in HIV infection is awaited.

ACKNOWLEDGEMENTS

The authors thanks the many scientists who have helped with their work over the years, especially N. Yamamoto and H. Mizusawa for discussions. Research in the authors' laboratory is supported by grants from the Ministry of Health, Labor, and Welfare and the Ministry of Education, Culture, Sports, Science, and Technology of Japan.

REFERENCES

1. Badley AD, Roumier T, Lum JJ, *et al.* Mitochondrion-mediated apoptosis in HIV-1 infection. *Trends Pharmacol Sci* 2003; **24**: 298–305.
2. Arnoult D, Petit F, Lelievre JD, *et al.* Mitochondria in HIV-1-induced apoptosis. *Biochem Biophys Res Commun* 2003; **304**: 561–574.
3. Lifson JD, Reyes GR, McGrath MS, *et al.* AIDS retrovirus induced cytopathology: giant cell formation and involvement of CD4 antigen. *Science* 1986; **232**: 1123–1127.
4. Terai C, Kornbluth RS, Pauza CD, *et al.* Apoptosis as a mechanism of cell death in cultured T lymphoblasts acutely infected with HIV-1. *J Clin Invest* 1991; **87**: 1710–1715.
5. Rinfret A, Latendresse H, Lefebvre R, *et al.* Human immunodeficiency virus-infected multinucleated histiocytes in oropharyngeal lymphoid tissues from two asymptomatic patients. *Am J Pathol* 1991; **138**: 421–426.
6. Frankel SS, Wenig BM, Burke AP, *et al.* Replication of HIV-1 in dendritic cell-derived syncytia at the mucosal surface of the adenoid. *Science* 1996; **272**: 115–117.
7. Sodroski J, Goh WC, Rosen C, *et al.* Role of the HTLV-III/LAV envelope in syncytium formation and cytopathicity. *Nature* 1986; **322**: 470–474.
8. Ferri KF, Jacotot E, Blanco J, *et al.* Apoptosis control in syncytia induced by the HIV type 1-envelope glycoprotein complex: role of mitochondria and caspases. *J Exp Med* 2000; **192**: 1081–1092.
9. Castedo M, Roumier T, Blanco J, *et al.* Sequential involvement of Cdk1, mTOR and p53 in apoptosis induced by the HIV-1 envelope. *EMBO J* 2002; **21**: 4070–4080.
10. Sastry KJ, Marin MC, Nehete PN, *et al.* Expression of human immunodeficiency virus type I tat results in down-regulation of bcl-2 and induction of apoptosis in hematopoietic cells. *Oncogene* 1996; **13**: 487–493.
11. Bartz SR, Emerman M. Human immunodeficiency virus type 1 Tat induces apoptosis and increases sensitivity to apoptotic signals by up-regulating FLICE/caspase-8. *J Virol* 1999; **73**: 1956–1963.
12. Jacotot E, Ravagnan L, Loeffler M, *et al.* The HIV-1 viral protein R induces apoptosis via a direct effect on the mitochondrial permeability transition pore. *J Exp Med* 2000; **191**: 33–46.
13. Green DR, Droin N, Pinkoski M. Activation-induced cell death in T cells. *Immunol Rev* 2003; **193**: 70–81.
14. Muro-Cacho CA, Pantaleo G, Fauci AS. Analysis of apoptosis in lymph nodes of HIV-infected persons. Intensity of apoptosis correlates with the general state of activation of the lymphoid tissue and not

with stage of disease or viral burden. *J Immunol* 1995; **154**: 5555–5566.
15. Finkel TH, Tudor-Williams G, Banda NK, *et al.* Apoptosis occurs predominantly in bystander cells and not in productively infected cells of HIV- and SIV-infected lymph nodes. *Nat Med* 1995; **1**: 129–134.
16. Suda T, Takahashi T, Golstein P, *et al.* Molecular cloning and expression of the Fas ligand, a novel member of the tumor necrosis factor family. *Cell* 1993; **75**: 1169–1178.
17. Medema JP, Scaffidi C, Kischkel FC, *et al.* FLICE is activated by association with the CD95 death-inducing signaling complex (DISC). *EMBO J* 1997; **16**: 2794–2804.
18. Medema JP, Toes RE, Scaffidi C, *et al.* Cleavage of FLICE (caspase-8) by granzyme B during cytotoxic T lymphocyte-induced apoptosis. *Eur J Immunol* 1997; **27**: 3492–3498.
19. Cohen GM. Caspases: the executioners of apoptosis. *Biochem J* 1997; **326**: 1–16.
20. Duan H, Dixit VM. RAIDD is a new 'death' adaptor molecule. *Nature* 1997; **385**: 86–89.
21. Yang X, Khosravi-Far R, Chang HY, *et al.* Daxx, a novel Fas-binding protein that activates JNK and apoptosis. *Cell* 1997; **89**: 1067–1076.
22. Sharma K, Wang RX, Zhang LY, *et al.* Death the Fas way: regulation and pathophysiology of CD95 and its ligand. *Pharmacol Ther* 2000; **88**: 333–347.
23. Newell MK, Desbarats J. Fas ligand: receptor or ligand? *Apoptosis* 1999; **4**: 311–315.
24. Bellgrau D, Gold D, Selawry H, *et al.* A role for CD95 ligand in preventing graft rejection. *Nature* 1995; **377**: 630–632.
25. Griffith TS, Brunner T, Fletcher SM, *et al.* Fas ligand-induced apoptosis as a mechanism of immune privilege. *Science* 1995; **270**: 1189–1192.
26. Walsh K, Sata M. Negative regulation of inflammation by Fas ligand expression on the vascular endothelium. *Trends Cardiovasc Med* 1999; **9**: 34–41.
27. Liles WC, Kiener PA, Ledbetter JA, *et al.* Differential expression of Fas (CD95) and Fas ligand on normal human phagocytes: implications for the regulation of apoptosis in neutrophils. *J Exp Med* 1996; **184**: 429–440.
28. Hsu H, Xiong J, Goeddel DV. The TNF receptor 1-associated protein TRADD signals cell death and NF-kappa B activation. *Cell* 1995; **81**: 495–504.
29. Wiley SR, Schooley K, Smolak PJ, *et al.* Identification and characterization of a new member of the TNF family that induces apoptosis. *Immunity* 1995; **3**: 673–682.
30. Cretney E, Uldrich AP, Berzins SP, *et al.* Normal thymocyte negative selection in TRAIL-deficient mice. *J Exp Med* 2003; **198**: 491–496.
31. Nitsch R, Bechmann I, Deisz RA, *et al.* Human brain-cell death induced by tumour-necrosis-factor-related apoptosis-inducing ligand (TRAIL). *Lancet* 2000; **356**: 827–828.
32. Mori E, Thomas M, Motoki K, *et al.* Human normal hepatocytes are susceptible to apoptosis signal mediated by both TRAIL-R1 and TRAIL-R2. *Cell Death Differ* 2004; **11**: 203–207.
33. Pan G, Ni J, Wei YF, *et al.* An antagonist decoy receptor and a death domain-containing receptor for TRAIL. *Science* 1997; **277**: 815–818.
34. Walczak H, Degli-Esposti MA, Johnson RS, *et al.* TRAIL-R2: a novel apoptosis-mediating receptor for TRAIL. *EMBO J* 1997; **16**: 5386–5397.
35. Almasan A, Ashkenazi A. Apo2L/TRAIL: apoptosis signaling, biology, and potential for cancer therapy. *Cytokine Growth Factor Rev* 2003; **14**: 337–348.
36. MacFarlane M. TRAIL-induced signalling and apoptosis. *Toxicol Lett* 2003; **139**: 89–97.
37. Pan G, O'Rourke K, Chinnaiyan AM, *et al.* The receptor for the cytotoxic ligand TRAIL. *Science* 1997; **276**: 111–113.
38. Sheridan JP, Marsters SA, Pitti RM, *et al.* Control of TRAIL-induced apoptosis by a family of signaling and decoy receptors. *Science* 1997; **277**: 818–821.
39. Legembre P, Moreau P, Daburon S, *et al.* Potentiation of Fas-mediated apoptosis by an engineered glycosylphosphatidylinositol-linked Fas. *Cell Death Differ* 2002; **9**: 329–339.
40. Kischkel FC, Lawrence DA, Chuntharapai A, *et al.* Apo2L/TRAIL-dependent recruitment of endogenous FADD and caspase-8 to death receptors 4 and 5. *Immunity* 2000; **12**: 611–620.
41. Lin Y, Devin A, Cook A, *et al.* The death domain kinase RIP is essential for TRAIL (Apo2L)-induced activation of IkappaB kinase and c-Jun *N*-terminal kinase. *Mol Cell Biol* 2000; **20**: 6638–6645.
42. Leverkus M, Neumann M, Mengling T, *et al.* Regulation of tumor necrosis factor-related apoptosis-inducing ligand sensitivity in primary and transformed human keratinocytes. *Cancer Res* 2000; **60**: 553–559.
43. Griffith TS, Chin WA, Jackson GC, *et al.* Intracellular regulation of TRAIL-induced apoptosis in human melanoma cells. *J Immunol* 1998; **161**: 2833–2840.
44. MacFarlane M, Harper N, Snowden RT, *et al.* Mechanisms of resistance to TRAIL-induced apoptosis in primary B cell chronic lymphocytic leukaemia. *Oncogene* 2002; **21**: 6809–6818.
45. Ahmad M, Shi Y. TRAIL-induced apoptosis of thyroid cancer cells: potential for therapeutic intervention. *Oncogene* 2000; **19**: 3363–3371.
46. Lamhamedi-Cherradi SE, Zheng SJ, Maguschak KA, *et al.* Defective thymocyte apoptosis and accelerated autoimmune diseases in TRAIL-/- mice. *Nat Immunol* 2003; **4**: 255–260.

47. Chicheportiche Y, Bourdon PR, Xu H, *et al.* TWEAK, a new secreted ligand in the tumor necrosis factor family that weakly induces apoptosis. *J Biol Chem* 1997; **272**: 32401–32410.
48. Kitson J, Raven T, Jiang YP, *et al.* A death-domain-containing receptor that mediates apoptosis. *Nature* 1996; **384**: 372–375.
49. Marsters SA, Sheridan JP, Pitti RM, *et al.* Identification of a ligand for the death-domain-containing receptor Apo3. *Curr Biol* 1998; **8**: 525–528.
50. Chinnaiyan AM, O'Rourke K, Yu GL, *et al.* Signal transduction by DR3, a death domain-containing receptor related to TNFR-1 and CD95. *Science* 1996; **274**: 990–992.
51. Yoo YG, Lee MO. Hepatitis B virus X protein induces expression of Fas ligand gene through enhancing transcriptional activity of early growth response factor. *J Biol Chem* 2004; **279**: 36242–36249.
52. Ruggieri A, Murdolo M, Rapicetta M. Induction of FAS ligand expression in a human hepatoblastoma cell line by HCV core protein. *Virus Res* 2003; **97**: 103–110.
53. Vasilescu A, Heath SC, Diop G, *et al.* Genomic analysis of Fas and FasL genes and absence of correlation with disease progression in AIDS. *Immunogenetics* 2004; **56**: 56–60.
54. Sieg S, Smith D, Yildirim Z, *et al.* Fas ligand deficiency in HIV disease. *Proc Natl Acad Sci USA* 1997; **94**: 5860–5865.
55. Ohnimus H, Heinkelein M, Jassoy C. Apoptotic cell death upon contact of CD4+ T lymphocytes with HIV glycoprotein-expressing cells is mediated by caspases but bypasses CD95 (Fas/Apo-1) and TNF receptor 1. *J Immunol* 1997; **159**: 5246–5252.
56. Katsikis PD, Wunderlich ES, Smith CA, *et al.* Fas antigen stimulation induces marked apoptosis of T lymphocytes in human immunodeficiency virus-infected individuals. *J Exp Med* 1995; **181**: 2029–2036.
57. Medrano FJ, Leal M, Arienti D, *et al.* Tumor necrosis factor beta and soluble APO-1/Fas independently predict progression to AIDS in HIV-seropositive patients. *AIDS Res Hum Retroviruses* 1998; **14**: 835–843.
58. Dockrell DH, Badley AD, Villacian JS, *et al.* The expression of Fas Ligand by macrophages and its upregulation by human immunodeficiency virus infection. *J Clin Invest* 1998; **101**: 2394–2405.
59. Yang Y, Bailey J, Vacchio MS, *et al.* Retinoic acid inhibition of *ex vivo* human immunodeficiency virus-associated apoptosis of peripheral blood cells. *Proc Natl Acad Sci USA* 1995; **92**: 3051–3055.
60. Badley AD, McElhinny JA, Leibson PJ, *et al.* Upregulation of Fas ligand expression by human immunodeficiency virus in human macrophages mediates apoptosis of uninfected T lymphocytes. *J Virol* 1996; **70**: 199–206.
61. Westendorp MO, Frank R, Ochsenbauer C, *et al.* Sensitization of T cells to CD95-mediated apoptosis by HIV-1 Tat and gp120. *Nature* 1995; **375**: 497–500.
62. Banda NK, Bernier J, Kurahara DK, *et al.* Crosslinking CD4 by human immunodeficiency virus gp120 primes T cells for activation-induced apoptosis. *J Exp Med* 1992; **176**: 1099–1106.
63. Zauli G, Gibellini D, Secchiero P, *et al.* Human immunodeficiency virus type 1 Nef protein sensitizes CD4(+) T lymphoid cells to apoptosis via functional upregulation of the CD95/CD95 ligand pathway. *Blood* 1999; **93**: 1000–1010.
64. Li CJ, Friedman DJ, Wang C, *et al.* Induction of apoptosis in uninfected lymphocytes by HIV-1 Tat protein. *Science* 1995; **268**: 429–431.
65. Geleziunas R, Xu W, Takeda K, *et al.* HIV-1 Nef inhibits ASK1-dependent death signalling providing a potential mechanism for protecting the infected host cell. *Nature* 2001; **410**: 834–838.
66. Casella CR, Rapaport EL, Finkel TH. Vpu increases susceptibility of human immunodeficiency virus type 1-infected cells to fas killing. *J Virol* 1999; **73**: 92–100.
67. Baumler CB, Bohler T, Herr I, *et al.* Activation of the CD95 (APO-1/Fas) system in T cells from human immunodeficiency virus type-1-infected children. *Blood* 1996; **88**: 1741–1746.
68. Estaquier J, Tanaka M, Suda T, *et al.* Fas-mediated apoptosis of CD4+ and CD8+ T cells from human immunodeficiency virus-infected persons: differential *in vitro* preventive effect of cytokines and protease antagonists. *Blood* 1996; **87**: 4959–4966.
69. Katsikis PD, Garcia-Ojeda ME, Wunderlich ES, *et al.* Activation-induced peripheral blood T cell apoptosis is Fas independent in HIV-infected individuals. *Int Immunol* 1996; **8**: 1311–1317.
70. Petrovas C, Mueller YM, Katsikis PD. HIV-specific CD8+ T cells: serial killers condemned to die? *Curr HIV Res* 2004; **2**: 153–162.
71. Lum JJ, Schnepple DJ, Nie Z, *et al.* Differential effects of interleukin-7 and interleukin-15 on NK cell anti-human immunodeficiency virus activity. *J Virol* 2004; **78**: 6033–6042.
72. de Oliveira Pinto LM, Garcia S, Lecoeur H, *et al.* Increased sensitivity of T lymphocytes to tumor necrosis factor receptor 1 (TNFR1)- and TNFR2-mediated apoptosis in HIV infection: relation to expression of Bcl-2 and active caspase-8 and caspase-3. *Blood* 2002; **99**: 1666–1675.
73. Herbein G, Mahlknecht U, Batliwalla F, *et al.* Apoptosis of CD8+ T cells is mediated by macrophages through interaction of HIV gp120 with chemokine receptor CXCR4. *Nature* 1998; **395**: 189–194.

74. Zangerle R, Gallati H, Sarcletti M, *et al.* Tumor necrosis factor alpha and soluble tumor necrosis factor receptors in individuals with human immunodeficiency virus infection. *Immunol Lett* 1994; **41**: 229–234.
75. Kayagaki N, Yamaguchi N, Nakayama M, *et al.* Type I interferons (IFNs) regulate tumor necrosis factor-related apoptosis-inducing ligand (TRAIL) expression on human T cells: a novel mechanism for the antitumor effects of type I IFNs. *J Exp Med* 1999; **189**: 1451–1460.
76. Griffith TS, Wiley SR, Kubin MZ, *et al.* Monocyte-mediated tumoricidal activity via the tumor necrosis factor-related cytokine, TRAIL. *J Exp Med* 1999; **189**: 1343–1354.
77. Sedger LM, Shows DM, Blanton RA, *et al.* IFN-gamma mediates a novel antiviral activity through dynamic modulation of TRAIL and TRAIL receptor expression. *J Immunol* 1999; **163**: 920–926.
78. Vidalain PO, Azocar O, Lamouille B, *et al.* Measles virus induces functional TRAIL production by human dendritic cells. *J Virol* 2000; **74**: 556–559.
79. Jeremias I, Herr I, Boehler T, *et al.* TRAIL/Apo-2-ligand-induced apoptosis in human T cells. *Eur J Immunol* 1998; **28**: 143–152.
80. Katsikis PD, Garcia-Ojeda ME, Torres-Roca JF, *et al.* Interleukin-1 beta converting enzyme-like protease involvement in Fas-induced and activation-induced peripheral blood T cell apoptosis in HIV infection. TNF-related apoptosis-inducing ligand can mediate activation-induced T cell death in HIV infection. *J Exp Med* 1997; **186**: 1365–1372.
81. Miura Y, Misawa N, Maeda N, *et al.* Critical contribution of tumor necrosis factor-related apoptosis-inducing ligand (TRAIL) to apoptosis of human CD4+ T cells in HIV-1-infected hu-PBL-NOD-SCID mice. *J Exp Med* 2001; **193**: 651–660.
82. Lum JJ, Pilon AA, Sanchez-Dardon J, *et al.* Induction of cell death in human immunodeficiency virus-infected macrophages and resting memory CD4 T cells by TRAIL/Apo2l. *J Virol* 2001; **75**: 11128–11136.
83. Zhang M, Li X, Pang X, *et al.* Identification of a potential HIV-induced source of bystander-mediated apoptosis in T cells: upregulation of trail in primary human macrophages by HIV-1 tat. *J Biomed Sci* 2001; **8**: 290–296.
84. Yang Y, Tikhonov I, Ruckwardt TJ, *et al.* Monocytes treated with human immunodeficiency virus Tat kill uninfected CD4(+) cells by a tumor necrosis factor-related apoptosis-induced ligand-mediated mechanism. *J Virol* 2003; **77**: 6700–6708.
85. Miura Y, Koyanagi Y, Mizusawa H. TNF-related apoptosis-inducing ligand (TRAIL) induces neuronal apoptosis in HIV-encephalopathy. *J Med Dent Sci* 2003; **50**: 17–25.
86. Martinez-Lorenzo MJ, Anel A, Gamen S, *et al.* Activated human T cells release bioactive Fas ligand and APO2 ligand in microvesicles. *J Immunol* 1999; **163**: 1274–1281.
87. Musgrave BL, Phu T, Butler JJ, *et al.* Murine TRAIL (TNF-related apoptosis inducing ligand) expression induced by T cell activation is blocked by rapamycin, cyclosporin A, and inhibitors of phosphatidylinositol 3-kinase, protein kinase C, and protein tyrosine kinases: evidence for TRAIL induction via the T cell receptor signaling pathway. *Exp Cell Res* 1999; **252**: 96–103.
88. Tollefson AE, Toth K, Doronin K, *et al.* Inhibition of TRAIL-induced apoptosis and forced internalization of TRAIL receptor 1 by adenovirus proteins. *J Virol* 2001; **75**: 8875–8887.
89. Kotelkin A, Prikhod'ko EA, Cohen JI, *et al.* Respiratory syncytial virus infection sensitizes cells to apoptosis mediated by tumor necrosis factor-related apoptosis-inducing ligand. *J Virol* 2003; **77**: 9156–9172.
90. Miura Y, Misawa N, Kawano Y, *et al.* Tumor necrosis factor-related apoptosis-inducing ligand induces neuronal death in a murine model of HIV central nervous system infection. *Proc Natl Acad Sci USA* 2003; **100**: 2777–2782.
91. Ryan LA, Peng H, Erichsen DA, *et al.* TNF-related apoptosis-inducing ligand mediates human neuronal apoptosis: links to HIV-1-associated dementia. *J Neuroimmunol* 2004; **148**: 127–139.

J. Biochem. **138**, 583–592 (2005)
doi:10.1093/jb/mvi158

Solution RNA Structures of the HIV-1 Dimerization Initiation Site in the Kissing-Loop and Extended-Duplex Dimers

Seiki Baba[1], Ken-ichi Takahashi[1,2], Satoko Noguchi[1], Hiroshi Takaku[1], Yoshio Koyanagi[3], Naoki Yamamoto[4] and Gota Kawai[1,*]

[1]Department of Life and Environmental Sciences, Chiba Institute of Technology, 2-17-1 Tsudanuma, Narashino, Chiba 275-0016; [2]Department of Bioscience, Faculty of Bioscience, Nagahama Institute of Bio-Science and Technology, 1266 Tamura-cho, Nagahama, Shiga 526-0829; [3]Institute for Virus Research, Kyoto University, Kyoto 606-8507; and [4]AIDS Research Center, The National Institute of Infectious Diseases, Toyama 1-23-1, Shinjuku-ku, Tokyo 162-8640

Received April 27, 2005; accepted August 13, 2005

Dimer formation of HIV-1 genomic RNA through its dimerization initiation site (DIS) is crucial to maintaining infectivity. Two types of dimers, the initially generated kissing-loop dimer and the subsequent product of the extended-duplex dimer, are formed in the stem-bulge-stem region with a loop including a self-complementary sequence. NMR chemical shift analysis of a 39mer RNA corresponding to DIS, DIS39, in the kissing-loop and extended-duplex dimers revealed that the three dimensional structures of the stem-bulge-stem region are extremely similar between the two types of dimers. Therefore, we designed two shorter RNA molecules, loop25 and bulge34, corresponding to the loop-stem region and the stem-bulge-stem region of DIS39, respectively. Based upon the chemical shift analysis, the conformation of the loop region of loop25 is identical to that of DIS39 for each of the two types of dimers. The conformation of bulge34 was also found to be the same as that of the corresponding region of DIS39. Thus, we determined the solution structures of loop25 in each of the two types of dimers as well as that of bulge34. Finally, the solution structures of DIS39 in the kissing-loop and extended-duplex dimers were determined by combining the parts of the structures. The solution structures of the two types of dimers were similar to each other in general with a difference found only in the A16 residue. The elucidation of the structures of DIS39 is important to understanding the molecular mechanism of the conformational dynamics of viral RNA molecules.

Key words: DIS, HIV-1, NMR, RNA, structure.

Abbreviations: DIS, dimerization initiation site; HIV-1, human immunodeficiency virus type 1.

Two molecules of viral genomic RNA are packaged in a dimeric state in the virion of human immunodeficiency virus type 1 (HIV-1), and this dimer formation is crucial to maintaining their infectivity (*1–4*). Accumulating evidence from both *in vivo* and *in vitro* experiments has shown that the specific sequence, the dimerization initiation site (DIS) located close to the 5′ terminus of the genomic RNA, is required for spontaneous dimerization of HIV-1 RNA. DIS can form a stem-loop structure with a self-complementary sequence in the loop and a bulge in the stem (*5*, *6*). The dimerization of DIS forms the kissing-loop dimer as the first step; then, their intramolecular stems are converted into intermolecular stems, generating the extended-duplex dimer (*7*, *8*). This two step dimerization process is called the kissing-loop mechanism. The kissing-loop dimer is converted into the extended-duplex dimer by incubation at 55°C (*9*, *10*) or by incubation at physiological temperature with the HIV-1 nucleocapsid protein, NCp7, which includes two basic regions and two zinc-fingers (*11*). A number of experiments have been performed to gain an understanding of the role of the zinc-fingers as well as the basic regions (*12–16*). Our previous results show that, for the two step dimerization from the kissing-loop dimer to the extended-duplex dimer, the two basic regions surrounding the N-terminal zinc finger of NCp7 have RNA chaperone activity by themselves, and the zinc fingers increase the efficiency of the activity (*17*, *18*).

A number of three dimensional structural analyses using NMR and X-ray methods have been performed to determine the conformation of each region of DIS, the loop region in the kissing-loop (*19*, *20*) or extended-duplex dimers (*21–24*), as well as the bulge-out region (*25–27*). However, our previous studies suggested that the 39mer RNA sequence, DIS39, which covers the entire bulge and loop regions, is necessary and sufficient for the two step dimerization (*28*, *29*). Thus, it is still relevant to determine the structures of the kissing-loop and extended-duplex dimers for DIS39 with the same sequence and conditions.

In the present study, we designed two shorter RNA molecules, loop25 and bulge34; loop25 includes the loop-stem region of DIS39, and bulge34 includes the stem-bulge-stem region (Fig. 1), respectively we then determined the solution structures of loop25 in each of the kissing-loop and extended-duplex dimers as well as bulge34. By combining the structure parts, the solution structures of DIS39 in the kissing-loop and extended-duplex dimers were able to be determined.

*To whom correspondence should be addressed. Tel/Fax: +81-47-478-0425, E-mail: gkawai@sea.it-chiba.ac.jp

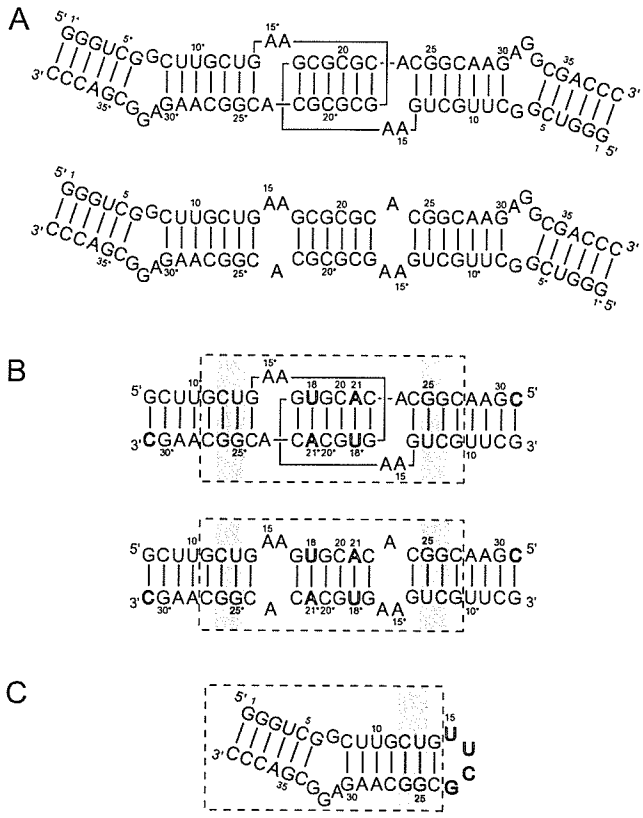

Fig. 1. **Secondary structure of a 39mer RNA corresponding to the dimerization initiation site (DIS39) and its fragments used in this study.** (A) The kissing-loop and extended-duplex dimers of DIS39. (B) The kissing-loop and extended-duplex dimers of loop25, which is composed of the loop and stem of DIS39. Modified residues are indicated by open characters. The sequence of the self-complementary loop was modified to increase the dispersion of NMR signals, and a base pair was added to the stem. The broken box indicates the part to be used for structure calculation. (C) Bulge34 consists of the stem-bulge-stem region of DIS39 and the connecting UUCG loop. The broken box indicates the part to be used for structure calculation. Gray shading indicates the two base pairs, C12–G26 and U13–G25, that are superimposed to combine the structures of the kissing-loop or extended-duplex dimer region and the stem-bulge-stem region. Asterisks indicate residues in the other strand.

MATERIALS AND METHODS

RNA Synthesis, Purification and Preparation—Nonlabeled loop25 was synthesized chemically by the phosphoramidite method with an automatic DNA/RNA synthesizer, Expedite model 8909 (PerSeptive Biosystems Inc., MA, USA). The protection groups were removed with ammonia and tetra-*n*-butylammonium fluoride. Nonlabeled DIS39 and bulge34 were synthesized enzymatically by the *in vitro* transcription reaction method with AmpliScribe T7 transcription kits (Epicentre Technologies Co., WI, USA). Purification for each RNA sample was performed by PAGE using 30 cm × 40 cm glass plates (Nihon Eido Co. Ltd., Tokyo, Japan) under denaturing conditions, and extensive desalting by ultrafiltration (Centricon YM3, Amicon Inc., MA, USA) was carried out. For stable isotopic labeling by the *in vitro* transcription with ^{13}C- and ^{15}N-labeled NTPs (Nippon Sanso, Tokyo, Japan), we used DIS39 rather than shorter loop25 and bulge34 because the efficiency of *in vitro* transcription is better for larger RNA.

For the preparation of the kissing-loop dimer, DIS39 or loop25 in water was incubated at 368 K for 5 min and chilled on ice for 5 min. Then, the solvent was adjusted to 1× PN-buffer [10 mM sodium phosphate (pH 7.0) and 50 mM NaCl] by adding concentrated buffer. For the preparation of the extended-duplex dimer, DIS39 or loop25 in 1× PN-buffer was incubated at 368 K for 5 min and slowly cooled to room temperature. Bulge34 was annealed by heating at 363 K for 5 min and snap-cooling on ice. To confirm the formation of the hairpin structure, the samples were subjected to a native PAGE experiment. For NMR measurements, RNA samples were dissolved in 10 mM sodium phosphate buffer (pH 7.0) containing 50 mM NaCl. The final concentration of chemically synthesized loop25 was 1.8 mM. The concentrations of DIS39 and bulge34 (transcripts) were 1.0 and 0.5 mM, respectively. The concentration of the kissing-loop and extended-duplex dimers of [G-$^{13}C/^{15}N$] and [A-$^{13}C/^{15}N$] DIS39 were 0.4, 0.3, 0.2 and 0.1 mM, respectively.

NMR Measurements—NMR spectra were recorded on Bruker DRX-500 and DRX-600 spectrometers. Spectra were recorded at probe temperatures of 283 to 303 K and NMR data at 298 K were used for structure calculation. The imino proton signal of the G and U residues in H_2O were distinguished from each other by the HSQC selected and HSQC filtered 1D spectra measured with ^{13}C and ^{15}N-labeled DIS39. Exchangeable proton NOEs were determined by 2D NOESY in H_2O with a mixing time of 150 ms using the jump-and-return scheme and gradient pulses for water suppression. For resonance assignments, well-established procedures were used (*30*). The H2 protons of adenosine were assigned based on a 2D HSQC experiment with natural abundance ^{13}C. NOE distance restraints from non-exchangeable protons were obtained from 2D NOESY experiments (mixing times of 50, 100, 200, and 400 ms) in D_2O. The intensities of the NOEs between exchangeable protons were interpreted as distances of 2.1–5.0 Å. For loop25, distances were estimated by analyzing the initial slope of NOE intensities for mixing times of 25, 50, 100, 200 ms. Judgment of intermolecular NOE is described in the result section. Two restraints (>5 Å) were added to the distance restraints based on the absence of NOE cross peaks in the case of the kissing-loop dimer. For bulge34, the intensities of NOEs due to nonexchangeable protons were interpreted as distances with a margin of −1.5 to +1.5 Å for the 100 ms 2D NOESY and −1.0 to +2.0 Å for the 200 ms 2D NOESY. Two restraints (>5 Å) were added to the distance restraints based on the absence of NOE cross peaks. The formation of hydrogen binding of G:C, A:U or G:U base pairs is interpreted as distance constraints as 1.8–2.1 Å for hydrogen and acceptor atoms and 2.8–3.2 Å for donor and acceptor atoms; G11:C27 to G14:C24, G11*:C27* to G14*:C24* and G17:C22* to C22:G17* for loop25 in the kissing-loop dimer, G11:C27* to G14:C24*, G11*:C27 to G14*:C24 and G17:C22* to C22:G17* for loop25 in the extended-duplex dimer, and G1:C39 to C5:G35 and U9:A29 to G14:C24 for bulge34. Dihedral restraints were obtained as described below. The absence of crosspeaks between H1′–H2′ in the 2D TOCSY and DQF-COSY experiments was interpreted as the residue being in the C3′-*endo*

conformation. On the other hand, the presence of strong crosspeaks between H1′–H2′ in the 2D TOCSY and DQF-COSY experiments was interpreted as the residue being in the C2′-*endo* conformation. The correction of sugar puckering is interpreted as dihedral restraints for ν_2 as 40.00 ± 20.00° (C3′-*endo*) or −35.00 ± 20.00° (C2′-*endo*). Based on the sequential connectivity of the Watson-Crick and G-U base pairs, the RNA-A conformation was assumed for the stem region and dihedral restraints were introduced for backbone torsion angles (α, β, γ, δ, ε and ζ) as the ideal conformation with a margin of ±10.00°. For loop25 in the kissing-loop dimer, information about the C3′-*endo* conformation (G11–G14, G17–C27), the C2′-*endo* conformation (A16) and RNA-A conformation in the stem region (G11–U13, U18–A21, G25–C27) was used as the dihedral restraints. For loop25 of the extended-duplex dimer, information about the C3′-*endo* conformation (G11–G14, G17-C27) and RNA-A conformation in the stem region (G11–U13, U18–A21, G25–C27) was used as the dihedral restraints. For bulge34, the information about the C3′-*endo* conformation (G1–G14, C24–A31, C34–C39) and RNA-A conformation in the stem region (G1–C5, G11–G14, C24–C27, G35–C39) was used as the dihedral restraints.

Structure Calculation—A set of 100 structures was calculated using the simulated annealing protocol described below with the InsightII/Discover package, and the amber force field was used. The force constants were 100 kcal mol^{-1} $Å^{-2}$ for distance restraints and 100 kcal mol^{-1} rad^{-2} for dihedral restraints. The starting coordinates were randomized, and the randomized structures were heated to 2,000 K in 5 ps, and the temperature was kept to 2,000 K for another 5 ps. After that, all restraints were increased to full values in 20 ps, then, decreased to 1/10 of full values in 5 ps at 2,000 K. Van der Waals radii were increased from 0.1 to 0.825 in 20 ps at 2,000 K. All restraints were increased to full value again in 10 ps at 2,000 K. Scalings for non-bond interactions were increased to full value in the next 20 ps at 2,000 K, and the temperature was kept to 2,000 K for another 5 ps. Then, the temperature was gradually scaled to 300 K in 10 ps. After that, the structure was heated from 300 to 1,000 K in 5 ps, and the van der Waals radii were increased from 0.825 to 1 at 1,000 K, and then decreased from 1 to 0.825 at 1,000 K. An additional 5 ps of dynamics was performed at 1,000 K, and the temperature was gradually scaled to 300 K for 10 ps. A final minimization step was performed, which included a Lennard-Jones potential and electrostatic terms with a dielectric constant of 7. The ten final structures with the lowest total energies were chosen.

RESULTS AND DISCUSSION

Analysis of the NMR Spectra of DIS39, Loop25 and Bulge34—Our previous NMR study revealed that the two types of dimers of DIS39 prepared as described in "MATERIALS AND METHODS" correspond to the kissing-loop and extended-duplex dimers (*31*). NMR spectra of DIS39 in each of the kissing-loop and extended-duplex dimers were measured in D_2O, and the signals due to H1′, H6/H8 were assigned by the sequential assignment method (Fig. 2). Figure 3A shows the difference in the chemical shift of H1′, H6/H8 between the two types of dimers. It was found that the difference is concentrated in the loop region. Interestingly, structures of the stem-bulge-stem region of the kissing-loop and extended-duplex dimers were extremely similar, even though the stems are formed by intra and inter molecules. This was also shown by analysis of the TOCSY spectrum; differences are located in the loop regions. Most residues were adapted to the C3′-*endo* conformation except for G32, G33 in the bulge-out region of both forms, A16 in the kissing-loop dimer and A15, A16 in the extended-duplex dimer, which might be a mixture of the C2′-*endo* and C3′-*endo* conformations.

To reveal further authentic structure, two RNA molecules were designed; loop25 includes the loop region and bulge34 includes the stem-bulge-stem region (Fig. 1, B and C). Loop25 was constructed to determine the authentic structure of the loop region. In order to increase the dispersion of the NMR signals, the sequence of the loop was modified from GCGCGC to GUGCAC. One base pair was added by replacing A31 by C31 in the stem to increase the stability of the kissing-loop dimer. It is noted that the loop sequences of GCGCGC and GUGCAC correspond to those of HIV-1 subtypes B and F (*32*), respectively, and both sequences have dimerization activity (*6*, *9*, *10*). The chemical shifts of loop25 were compared with those of DIS39 in each of the kissing-loop and extended-duplex dimers (Fig. 3, B and C). For both conformations, the chemical shifts for most of the stem region and A15, A16 and A23 were strikingly similar between the loop25 and DIS39. Due to the base alterations, the chemical shifts of the self complement loop were slightly different for both dimers. The chemical shift of H8 was shifted more than 0.2 ppm due to the addition of the terminal base pair. It is noteworthy that the chemical shift difference in loop25 between the kissing-loop and extended-duplex dimers (Fig. 3D) was almost identical to that of DIS39 (Fig. 3A). These results indicate that the structures of loop25 in the kissing-loop and extended-duplex dimers are essentially identical to those of DIS39. Upon analysis of the TOCSY spectrum, it was found that most of the residues were adapted to the C3′-*endo* conformation except A15 and A16 for the extended duplex dimer and A16 for the kissing loop dimer, and these results also agree with the results for DIS39.

Bulge34 was constructed to determine the authentic structure of the stem-bulge-stem region. Bulge34 consists of the stem-bulge-stem region of DIS39 and the connecting UUCG loop. The NMR signals of bulge34 were assigned by the sequential assignment technique. The chemical shift of H1′, H6/H8 of bulge34 were compared to those of DIS39 in the kissing-loop dimer (Fig. 3E). The chemical shifts for the stem-bulge-stem regions of bulge34 and DIS39 were identical, although the chemical shifts of the residues adjacent to the loop were slightly different by reflecting the difference in the closing loop sequences. Upon analysis of the TOCSY spectrum, it was found that most residues were adapted to the C3′-*endo* conformation except for G32, G33 in the bulge-out region and C in the UUCG loop, and that the conformation in the stem-bulge-stem region also agreed with that of DIS39. These results indicate that the structure of the stem-bulge-stem region of bulge34 is identical to that of DIS39.

Thus, the structures of DIS39 for two types of dimers can be determined by determining the structures of loop25 and bulge34, and combining them.

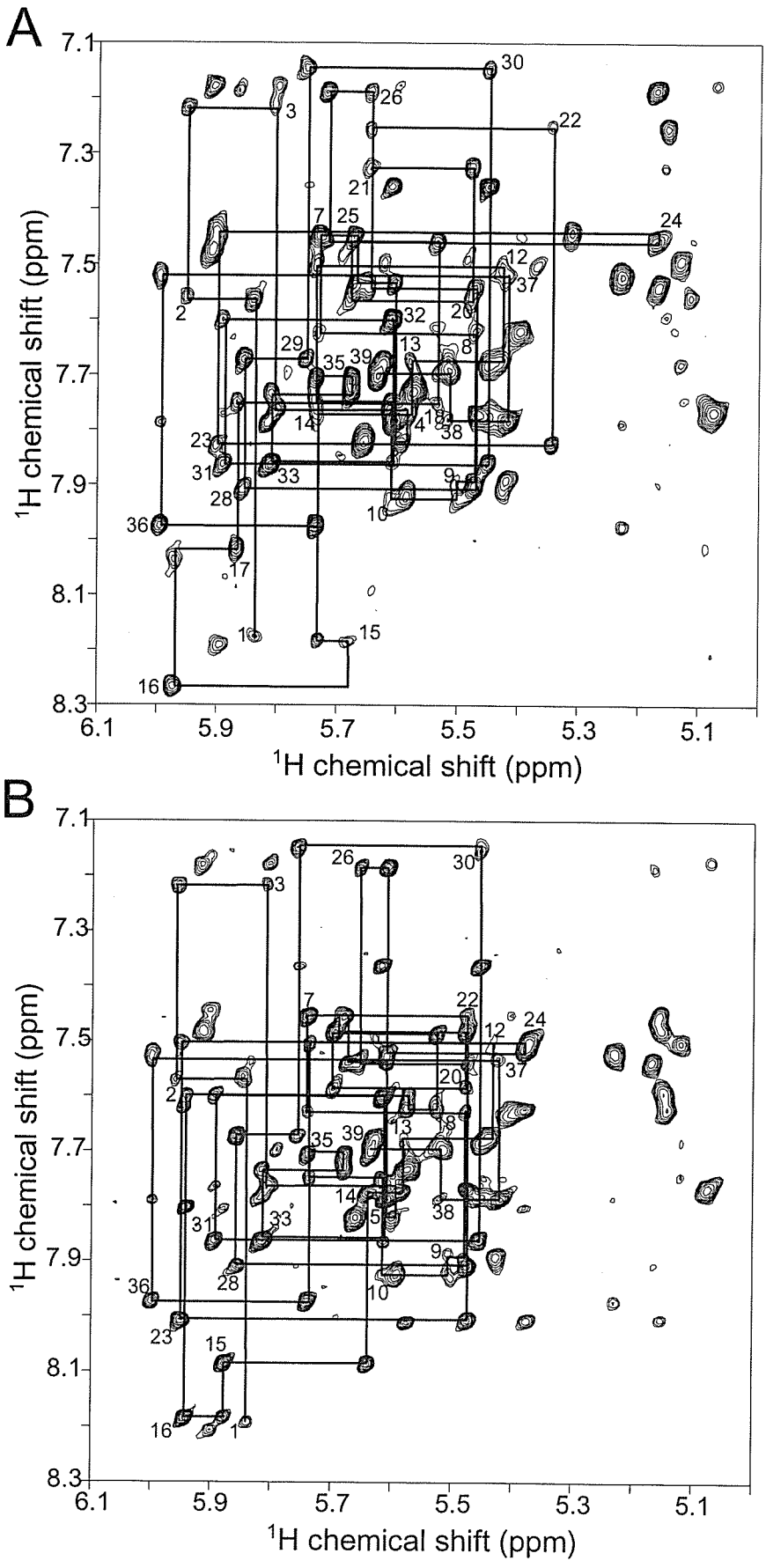

Fig. 2. **2D NOESY spectra of the (A) kissing-loop and (B) extended-duplex dimers of DIS39 measured in D_2O at 25°C with a mixing time of 200 ms.** Cross-peaks between aromatic H6/H8 protons and ribose H1′ protons are shown, and the sequential NOE connectivity is indicated.

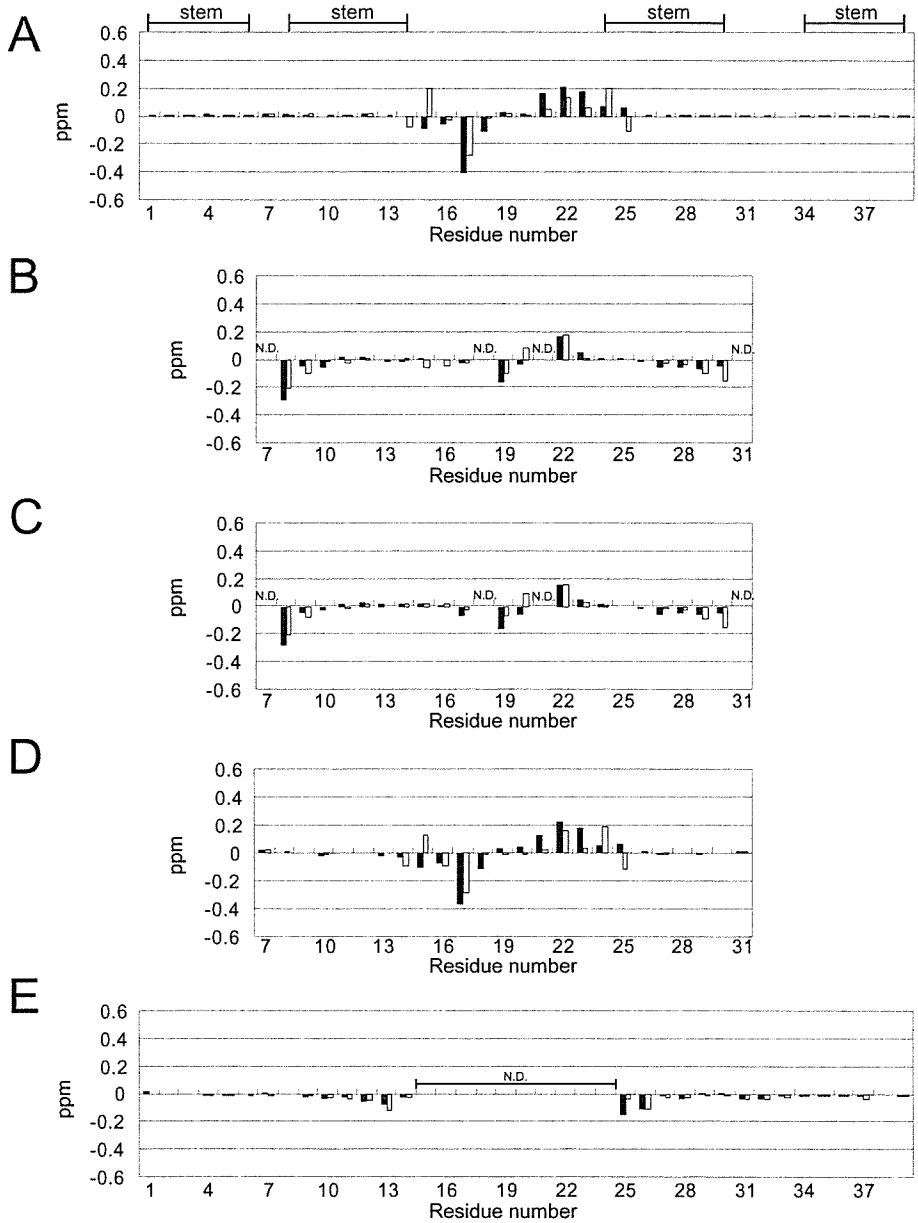

Fig. 3. **Chemical shift differences for H6/H8 and H1′.** Filled and open bars indicate H6/H8 and H1′, respectively. (A) Chemical shift differences between the kissing-loop and extended-duplex dimers of DIS39. Lines above the graph indicate the stem regions. (B) Chemical shift differences between DIS39 and loop25 in the kissing-loop dimer (data for replaced residues 7, 18, 21 and 31 are not shown). (C) Chemical shift differences between DIS39 and loop25 in the extended-duplex dimer (data for replaced residues 7, 18, 21 and 31 are not shown). (D) Chemical shift differences between the kissing-loop and extended-duplex dimers of loop25. (E) Chemical shift differences between DIS39 and bulge34 in the kissing-loop dimer (data for residues 15–24 are not shown).

Structure Determination—The loop region of loop25 in the kissing-loop dimer: To determine the structure of the loop region of DIS39 in both the kissing-loop and extended-duplex dimers, the NMR signals of loop25 were further analyzed and structural information was collected. The structure of the loop region consisting of the nine nucleotide loop and the stem with four base pairs was determined as shown by the broken box in Fig. 1B. A total of 286 distance restraints, 76 hydrogen bonding distance restraints, 140 dihedral restraints (Table 1), and 136 chiral restraints were used for the structural calculation. Three NOEs in the loop region, H2(A21)–H1′(U18), H2(A21)–H1′(G19) and H2(A21)–H8(G19), were judged to be intermolecular by analysis of the imino proton spectra. Four NOEs in the stem-loop linking region were considered to be intermolecular or intramolecular based on the results of the isotope filter NMR measurement (data not shown), and it was concluded that two NOEs, H2(A23)–H1′ (G17), H2(A16)–H1′ (G16), are intermolecular and three NOE, H8(A16)–H1′ (A16), H8(A16)–H2′ (A16), are intramolecular. One NOE in the stem-loop linking region was considered to be intermolecular or intramolecular in the structure calculation, and it was concluded that this NOE, H2(A23)–H2(A15), is intramolecular. Each restraint is used twice for two molecules. The structures were calculated by the restrained molecular dynamic calculation with the simulated annealing method. The structure was defined with a heavy atom r.m.s.d. of 2.14 Å for the ten converged structures (Fig. 4A, left panel), and the minimized average structure is shown in Fig. 4A (right panel). Although the overall convergence was not very good, the self-complementary region was well defined with 0.76 Å, and the stem-loop linking region was defined with 1.86 Å. The structural statistics are summarized in Table 1.

The loop region of loop25 in the extended-duplex dimer: The loop region of loop25 in the extended-duplex dimer was

Table 1. **NMR restraints and structural statistics.**

	Number of restraints		
	loop25 in the kissing-loop dimer (17 mer × 2)	loop25 in the extended-duplex dimer (17 mer × 2)	bulge34 (30 mer)
Distance restraints	286	384	345
imino-imino	12	12	10
intra residue	154	182	163
intra molecule	106	174	170
inter molecule	12	16	–
>5 Å	2	0	2
Hydrogen bonding distance restraints	76	76	58
Dihedral restraints	140	138	126
3′-*endo*	30	30	28
2′-*endo*	2	0	0
RNA-A stems	108	108	98
r.m.s.d. from the idealized geometry (Å)			
Bonds (Å)	0.00897 ± 0.00004	0.00803 ± 0.00020	0.00775 ± 0.00015
Angle (°)	2.43 ± 0.23	2.33 ± 0.05	2.24 ± 0.07
Impropers (°)	1.57 ± 0.10	1.82 ± 0.64	1.53 ± 0.21
Heavy-atoms r.m.s.d. (Å)[a]			
All	2.14	1.45	1.98
Stem-loop linking region[b]	1.86	1.31	
Bulge region[c]			1.90

[a]Averaged r.m.s.d. between an average structure and the 10 converged structures were calculated. The converged structures did not contain experimental distance violations >0.2 Å or dihedral violations >5°, [b]The stem-loop linking region consists of residues 14 to 17, 22 to 24, 14* to 17* and 22* to 24*, [c]The bulge region consists of residues 6 to 10 and 28 to 34. Asterisks indicate residues in the other molecule.

determined (broken box in Fig. 1B). A total of 384 distance restraints, 76 hydrogen bonding distance restraints, 138 dihedral restraints (Table 1) and 136 chiral restraints were used for the structure calculation. For the stem-loop linking region, H2 of A23 was connected by intermolecular NOEs to H1′ and H2 of A15, H2 of A16 and H1′ of G17. The structures were calculated by the restrained molecular dynamic calculation with the simulated annealing method described above. The structure was well defined with a heavy atom r.m.s.d. of 1.45 for the ten converged structures (Fig. 4B, left panel), and the minimized average structure is shown in Fig. 4B (right panel). The stem-loop linking region was defined with 1.31 Å. The structural statistics are summarized in Table 1.

The stem-bulge-stem region of bulge34: A structural determination was performed for bulge34 except for the UUCG loop (broken box in Fig. 1C). A total of 345 distance restraints, 58 hydrogen bonding distance restraints, 126 dihedral restraints (Table 1) and 120 chiral restraints were used for the structure calculation. Two NOE restraints (>5 Å), H2(A31)–H1′(U9) and H1′(A31)–H1′(U9), were added to the distance restraints based on the absence of NOE cross peaks. The structures were calculated by the restrained molecular dynamic calculation with a simulated annealing protocol. The structure was defined with a heavy atom r.m.s.d. of 1.98 for the ten converged structures (Fig. 4C, left panel), and the minimized average structure is shown in Fig. 4C (right panel). Although the overall convergence is not very good, the stem regions are well defined with 0.83 or 0.78 Å, respectively. The bulge region was defined with 1.90 Å. The structural statistics are summarized in Table 1.

The two types of dimers of DIS39: Solution structures of DIS39 were then constructed by combining the structure parts. The structures of the kissing-loop or extended-duplex dimer region and stem-bulge-stem region were combined by superimposing two base pairs, C12:G26 and U13:G25 (Fig. 1, gray area). The left panels of Fig. 5 show the ten structures prepared by using the minimized average structure of the stem-bulge-stem region (Fig. 4C, right) and each of the ten lowest energy structures of the loop region (Fig. 4, A or B, left) superimposed by the loop region. The right panels of Fig. 5 show the structures prepared using the minimized average structure of the stem-bulge-stem region (Fig. 4C, right) and the loop region (Fig. 4, A or B, right). The relative angles between the stem-bulge-stem regions differ between the kissing-loop and extended-duplex dimers as shown in the right panels of Fig. 5. However, the fluctuations of the relative angles are rather large and the ranges overlap between the two dimers as shown in the left panels of Fig. 5. In fact, the values of the residual dipolar coupling for the stem-bulge-stem region are similar between the kissing-loop and extended-duplex dimers (to be published). A preliminary normal mode analysis suggested the existence of hinge motion, and, in order to reveal the dynamic properties of the dimers, a molecular dynamics analysis, as well as the thermodynamics analysis (*33*), is required. The most obvious local difference was observed for A16; for the kissing-loop dimer, A16 was close to the same residue in the other molecule (Fig. 6A, left) and did not stack above A15 of the same molecule nor G17 of the other molecule (Fig. 6A, right), whereas for the extended-duplex dimer, A16 was apart from the same residue of the other molecule (Fig. 6B, left) and stacked between A15 and G17 (Fig. 6B, right).

Structural Comparison with Related Structures—Ennifar *et al.* (*20*) determined the crystal structure of

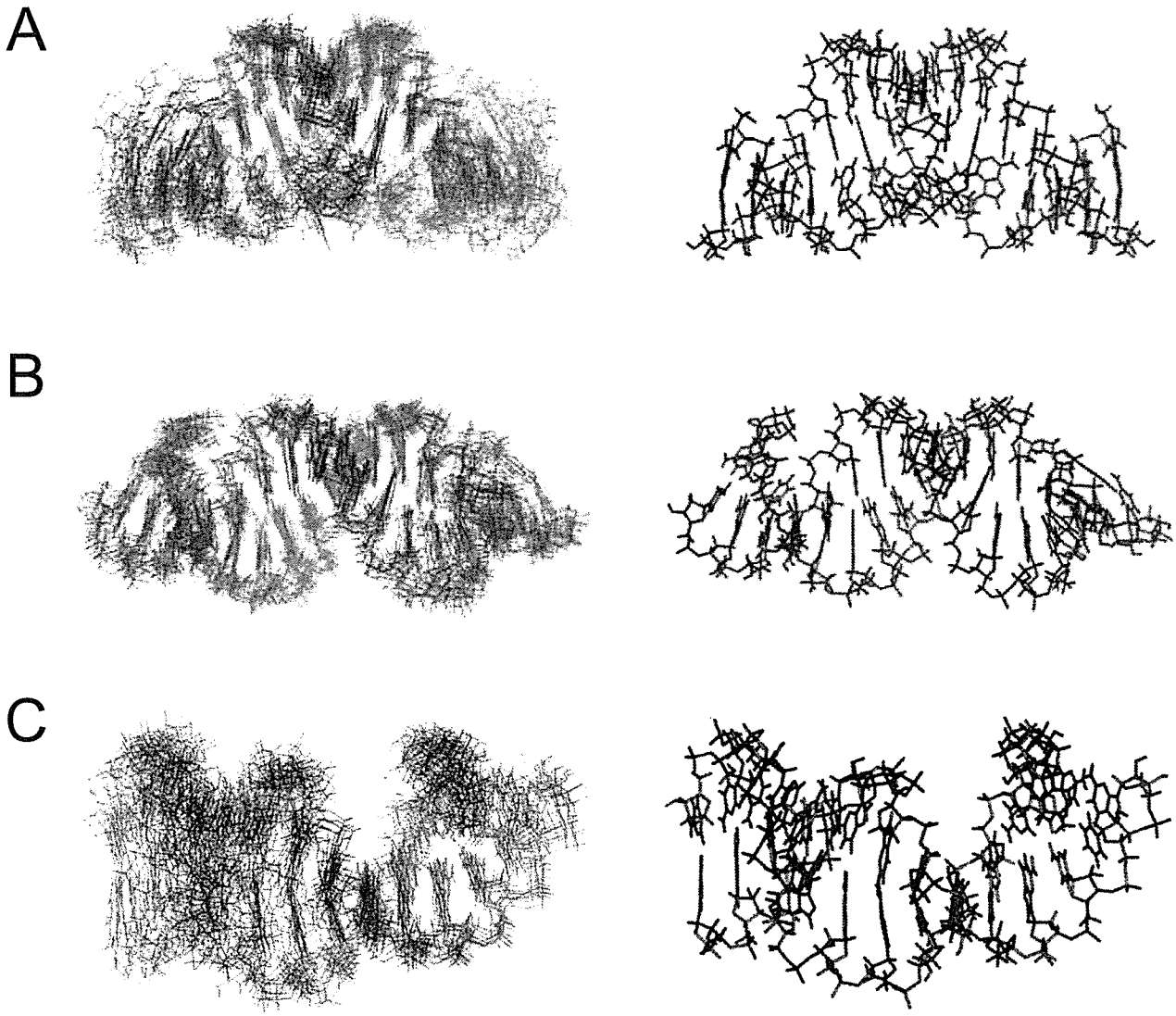

Fig. 4. **Solution structures of each part of DIS39.** Left panels show the superimposition of the 10 lowest energy structures and the right panels show the minimized average structures. (A) The loop region of loop25, as shown by the broken box in Fig. 1b, in the kissing-loop dimer. Each strand is colored in red or blue. (B) The loop region of loop25 in the extended-duplex dimer. (C) The stem-bulge-stem region of bulge34.

the kissing-loop dimer. The present structure is similar to the crystal structures in general, except for A15 and A16. In the present structure, A15 stacks on G14 and A16 interacts with the same residue in the other molecule (Fig. 6A, right). On the other hand, in the crystal structure, A15 and G16 are flipped out (*20*). It is noted that the numbering system of DIS39 is used for other structures for convenience, and position 16 is occupied by A or G depending on the strain. A15 and A16 (or G16) might be flexible and can be flipped out even in solution. Mujeeb *et al.* (*19*) determined the solution structure of the kissing-loop dimer. In this structure, A16 interacts with A15 and C24 in the other molecule, and, as a result, the distance between the two stems is relatively short. Thus, this restricted interaction makes the global structure different from the present structure and the crystal structure. However, the location of A15 is similar in the two solution structures. The difference in the conformation of A16 between the two solution structures may reflect the difference in the sequence of the stem adjacent to the loop and/or in the sample condition, including the salt concentration. The NOE connectivity determined in the present study agrees in general with those of Dardel *et al.* who analyzed the structure of the stem-loop region in the kissing-loop dimer by NMR (*34*).

Girard *et al.* (*21*) and Mujeeb *et al.* (*22*) determined the solution structures of extended-duplex dimers. In these two structures, as well as in the present structure, A15, A16 and A23 form a zipper like structure (Fig. 6B, right). On the other hand, in the case of the crystal structure of the extended-duplex dimer, G16 forms a G:A base pair and A15 is flipped out, and it was assumed that this in-out bulge transconformation is magnesium-dependent (*23*).

Structures of the stem-bulge-stem region were shown by Lawrence *et al.* (*26*) and Yuan *et al.* (*27*). In the solution structure determined by Lawrence *et al.* (*26*), continuous stackings were formed for each strand, G6-C8 and

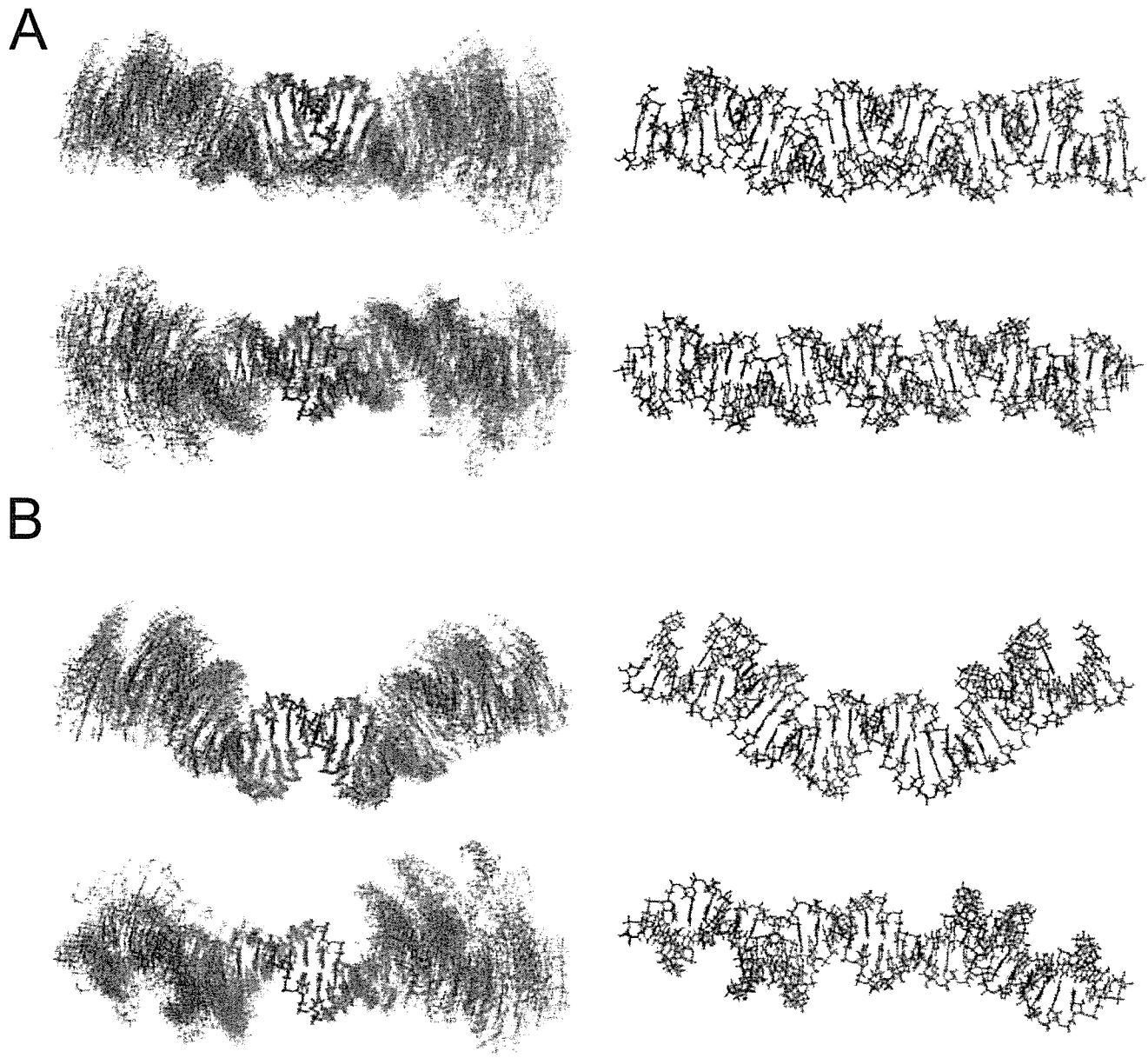

Fig. 5. **Solution structures of the (A) kissing-loop and (B) extended-duplex dimers of DIS39.** Left panels show the structures constructed by combining the structures of the loop (the 10 lowest energy structures of the kissing-loop or extended-duplex dimers) and the stem-bulge-stem (minimized average structure) regions. Right panels show the structures constructed by combining the minimized average structures of the loop and stem-bulge-stem regions. The two regions were combined by superimposing two base pairs, C12–G26 and U13–G25 (Fig. 1, gray area). Each strand is colored in red or blue and views from two different directions are shown.

G30-C34. Yuan *et al.* (*27*) showed that G7 and A31 form a base pair, and that G33 is not always stacked on G32 or C34, and, in general, the present structure is identical to the latter structure. Greatorex *et al.* (*25*) showed that the bulge region is too flexible to determine the conformation. These conformational differences may be caused by differences in the stability of the terminal stem. Lawrence *et al.* (*26*) adopted a stable 7 base-pair stem, and their structure forms an ordered conformation in the bulge region. In contrast, Greatorex *et al.* (*25*) adopted an unstable 4 base-pair stem and the bulge region is flexible. Yuan *et al.* (*27*) adopted a 4 base-pair stem and a flanking adenosine residue at the 3′ terminal that must stabilize the stem. In the present study, a 6 base-pair stem was used.

Mechanism of the Two Stem Dimerization—Between the kissing-loop and extended-duplex dimers, A16 shows the most drastic change in interaction with other residues, suggesting that A16 is the key residue in the two step dimerization reaction. The difference in the A16 conformation among structures with different sequences and determined under different conditions as described above, also suggests the importance of this residue. Mujeeb *et al.* (*19*, *22*) also pointed out the flexibility around the junction of the loop and the stem of DIS in the kissing-loop and